

Response of thin-film SQUIDs to applied fields and vortex fields: Linear SQUIDs

John R. Clem

Ames Laboratory - DOE and Department of Physics and Astronomy, Iowa State University, Ames Iowa 50011

Ernst Helmut Brandt

Max-Planck-Institut für Metallforschung, D-70506 Stuttgart, Germany

(Dated: October 29, 2018)

In this paper we analyze the properties of a dc SQUID when the London penetration depth λ is larger than the superconducting film thickness d . We present equations that govern the static behavior for arbitrary values of $\Lambda = \lambda^2/d$ relative to the linear dimensions of the SQUID. The SQUID's critical current I_c depends upon the *effective flux* Φ , the magnetic flux through a contour surrounding the central hole plus a term proportional to the line integral of the current density around this contour. While it is well known that the SQUID inductance depends upon Λ , we show here that the focusing of magnetic flux from applied fields and vortex-generated fields into the central hole of the SQUID also depends upon Λ . We apply this formalism to the simplest case of a linear SQUID of width $2w$, consisting of a coplanar pair of long superconducting strips of separation $2a$, connected by two small Josephson junctions to a superconducting current-input lead at one end and by a superconducting lead at the other end. The central region of this SQUID shares many properties with a superconducting coplanar stripline. We calculate magnetic-field and current-density profiles, the inductance (including both geometric and kinetic inductances), magnetic moments, and the effective area as a function of Λ/w and a/w .

PACS numbers: **74.78.-w**

I. INTRODUCTION

The research in this paper has been motivated by several important recent developments in superconductivity: (a) the fabrication of thin-film SQUIDs (superconducting quantum interference devices) made of high- T_c superconductors,¹ (b) the study of noise generated by vortices in active and passive superconducting devices,^{1,2,3,4,5,6,7,8,9,10} and (c) line-width reduction in superconducting devices to eliminate noise due to vortices trapped during cooldown in the earth's magnetic field.^{11,12,13,14,15,16}

The fact that the London penetration depth λ increases as T increases and diverges at T_c is an important consideration for high- T_c SQUIDs operated at liquid-nitrogen temperature. When λ is larger than the film thickness d , the physical length that enters the equations governing the spatial variation of currents and fields is the Pearl length¹⁷ $\Lambda = \lambda^2/d$. Accordingly, the equations governing the behavior of active or passive thin-film superconducting devices depend upon the ratio of Λ to the linear dimensions of the device. In particular, the equations governing SQUIDs involve not just the magnetic flux up through a contour within the SQUID, but the effective flux Φ , which is the sum of the magnetic flux and a term proportional to the line integral of the current density around the same contour. While the effective flux Φ is similar to London's fluxoid,¹⁸ which is quantized in multiples of the superconducting flux quantum $\phi_0 = h/2e$, we show in the next section that Φ is not quantized. We also give in Sec. II the basic equations, valid for any value of Λ , that govern the behavior of a dc SQUID.

A vortex trapped in the body of the SQUID during cooldown through the superconducting transition temperature T_c in an ambient magnetic field generates a magnetic field and a screening current that together make a sizable vortex-position-dependent contribution Φ_v to the effective flux Φ . If such a vortex remains fixed in position and the temperature remains constant, this simply produces a harmless bias in Φ . On the other hand, both vortex motion due to thermal agitation and temperature fluctuations generate corresponding fluctuations in Φ_v and noise in the SQUID output. In Sec. II we show that to calculate Φ_v , it is not necessary to calculate the spatial dependence of the vortex-generated fields and currents. Instead, one may determine Φ_v with the help of the sheet-current distribution of a circulating current in the absence of the vortex.

In Sec. III we apply the basic equations of Sec. II to calculate the properties of a model linear SQUID, which has the basic topology of a SQUID but is greatly stretched along one axis, such that the central portion resembles a coplanar stripline. The advantage of using such a model is that simple analytical results can be derived that closely approximate the exact numerically calculated quantities in the appropriate limits. In addition to calculating the field and current distributions for several values of Λ , we calculate the total inductance, geometric inductance, kinetic inductance, and magnetic moment when the SQUID carries a circulating current. We calculate the field and current distributions, magnetic moment, and effective area $A_{\text{eff}} = \Phi_f/B_a$ when a perpendicular magnetic induction B_a is applied and the effective flux Φ_f is focused into the SQUID. Finally, we calculate the field and current distributions and the magnetic moment for the zero-fluxoid state when the junctions are

short-circuited and the sample remains in the state with $\Phi = 0$ when a perpendicular magnetic induction B_a is applied.

In Sec. IV, we present a brief summary of our results.

II. BASIC EQUATIONS

Our purpose in this section is to derive general equations that govern the behavior of a dc SQUID consisting of thin superconducting films of thickness d less than the weak-field London penetration depth λ , such that the fields and currents are governed by the two-dimensional screening length or Pearl length¹⁷ $\Lambda = \lambda^2/d$. We calculate both the current $I = I_1 + I_2$ through the SQUID [see Fig. 1] and the circulating current¹⁹ $I_d = (I_2 - I_1)/2$ and describe how to calculate the critical current I_c of the SQUID for arbitrary values of the SQUID's inductance L . For this case, the contributions from line integrals of the current density to the *effective flux* in the hole cannot be neglected, and the kinetic inductance makes a significant contribution to L . When a perpendicular magnetic induction B_a is applied, we calculate how much magnetic flux is focused into the SQUID's hole; this flux also can be expressed in terms of the effective area²⁰ of the hole. We also show how to calculate how much magnetic flux generated by a vortex in the main body of the SQUID is focused into the hole.

Consider a dc SQUID in the xy plane, as sketched in Fig. 1. We suppose that the SQUID is symmetric about the y axis, which lies along the centerline. The maximum Josephson critical current is I_0 for each of the Josephson junctions, shown as small black squares. The currents up through the left and right sides of the SQUID can be written as $I_1 = I/2 - I_d$ and $I_2 = I/2 + I_d$. When the magnitude of I , the total current through the SQUID, is less than the critical current I_c , the equations that determine $I = I_1 + I_2$ and the circulating current $I_d = (I_2 - I_1)/2$ can be derived using a method similar to that used in Ref. 21. We begin by writing the local current density \mathbf{j} in the superconductors (i.e., the main body of the SQUID and the counterelectrode) as¹⁸

$$\mathbf{j} = -(1/\mu_0\lambda^2)[\mathbf{A} + (\phi_0/2\pi)\nabla\gamma], \quad (1)$$

where \mathbf{A} is the vector potential, $\phi_0 = h/2e$ is the superconducting flux quantum, and γ is the phase of the order parameter. The quantity inside the brackets, which is gauge-invariant, can be thought of as the superfluid velocity expressed in units of vector potential. From the point of view of the Ginzburg-Landau theory, implicit in the use of this London-equation approach is the assumption that the applied fields and currents are so low that the magnitude of the order parameter is not significantly reduced from its equilibrium value in the absence of fields and currents.

To obtain the SQUID equations, we integrate the vector potential around a contour C that passes in a counterclockwise direction through both junctions, the main

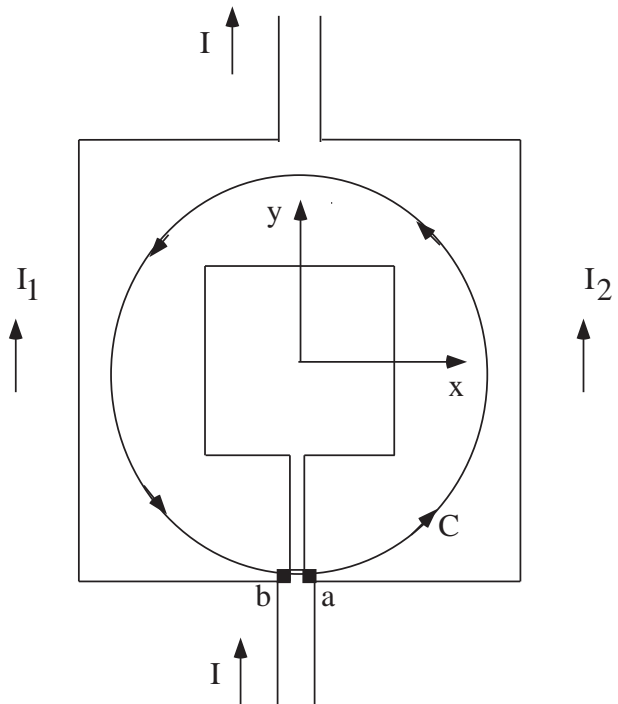


FIG. 1: I enters the main body of the SQUID from the counterelectrode below through two Josephson junctions (small black squares, labeled a and b) and divides into the currents $I_1 = I/2 - I_d$ and $I_2 = I/2 + I_d$ as shown.

body of the SQUID, and the counterelectrode as shown in Fig. 1 and write the result in two ways. Since $\mathbf{B} = \nabla \times \mathbf{A}$, this integral yields, on the one hand, the magnetic flux in the z direction

$$\int_S B_z(x, y) dS, \quad (2)$$

where S is the area surrounded by the contour C and $B_z(x, y)$ is the z component of the net magnetic induction in the plane of the SQUID produced by the sum of a perpendicular applied field B_a and the self-field $B_{sz}(x, y)$ generated via the Biot-Savart law by the supercurrent density $\mathbf{j}(x, y)$. On the other hand, for those portions of the contour lying in the superconductors, we eliminate the line integrals of \mathbf{A} in favor of line integrals of \mathbf{j} using Eq. (1). We then express the line integrals of $\nabla\gamma$ in terms of the values of γ at the junctions. Equating the two expressions for the line integral of \mathbf{A} , we find that the *effective flux* Φ in the z direction through the SQUID is given by

$$\Phi = (\phi_0/2\pi)(\phi_1 - \phi_2), \quad (3)$$

where

$$\Phi = \int_S B_z(x, y) dS + \mu_0\lambda^2 \int_C \mathbf{j} \cdot d\mathbf{l}, \quad (4)$$

with the integration contour C now passing through both superconductors but excluding the junction barriers. These equations are equivalent to Eq. (8.67) in

Ref. 21. The gauge-invariant phase differences across the junctions b and a are, respectively,²²

$$\phi_1 = \gamma_{bc} - \gamma_{bs} - (2\pi/\phi_0) \int_{bc}^{bs} \mathbf{A} \cdot d\mathbf{l}, \quad (5)$$

$$\phi_2 = \gamma_{ac} - \gamma_{as} - (2\pi/\phi_0) \int_{ac}^{as} \mathbf{A} \cdot d\mathbf{l}, \quad (6)$$

where bc labels a point on the counterelectrode side of the junction b and bs labels the point directly across the insulator in the SQUID washer, and ac and as label corresponding points for junction a . According to the Josephson equations,²² the junction supercurrents are $I_1 = I_0 \sin \phi_1$ and $I_2 = I_0 \sin \phi_2$. In the above derivation we have assumed that the linear dimensions of the Josephson junctions are much less than the Josephson penetration depth λ_J ,²² and that the applied fields are sufficiently small that the Josephson current densities and gauge-invariant phase differences are very nearly constant across the junction areas.

The magnetic moment $\mathbf{m} = m\hat{z}$ generated by the currents in the SQUID is²³

$$\mathbf{m} = \frac{1}{2} \int \mathbf{r} \times \mathbf{j} d^3r. \quad (7)$$

It can be shown with the help of the London fluxoid quantization condition,¹⁸

$$\int_{S'} B_z(x, y) dS + \mu_0 \lambda^2 \int_{C'} \mathbf{j} \cdot d\mathbf{l} = n\phi_0, \quad (8)$$

where n is an integer and C' is a closed contour that surrounds an area S' within the body of the SQUID, that if there are no vortices present (i.e., when $n = 0$), the expression for Φ in Eq. (4) is independent of the choice of contour C . Any convenient path can be chosen for C , provided only that the path remains in the superconducting material in the body of the SQUID and the counterelectrode. On the other hand, when there are vortices in the main body of the SQUID, the quantity Φ increases by ϕ_0 each time the contour C is moved from a path inside the vortex axis to one enclosing the vortex axis. Thus, without specifying the precise contour C , Φ is determined only modulo ϕ_0 . However, this is of no physical consequence, because the gauge-invariant phases ϕ_1 and ϕ_2 , which also enter Eq. (3), are also determined only modulo 2π . The final equations determining the currents I and I_d are independent of the choice of contour C and remain valid even when vortices are present in the main body of the SQUID.

When the thickness d of the SQUID is much larger than λ , the contours C and C' can be chosen to be at the midpoint of the thickness, where \mathbf{j} is exponentially small, such that the line integrals of \mathbf{j} can be neglected. The resulting equations are then the familiar ones found in many reference books, such as Refs. 21,24,25,26,27,28,29. However, we are interested here in the case for which $d < \lambda$, such that the fields and currents are governed by

the two-dimensional screening length or Pearl length¹⁷ $\Lambda = \lambda^2/d$. The term in Eq. (4) involving \mathbf{j} then must be carefully accounted for. For this case, \mathbf{j} is very nearly constant over the thickness and it is more convenient to deal with the sheet-current density $\mathbf{J}(x, y) = \mathbf{j}d$, such that Eqs. (4) and (8) take the form³⁰

$$\Phi = \int_S B_z(x, y) dS + \mu_0 \Lambda \int_C \mathbf{J} \cdot d\mathbf{l} \quad (9)$$

and

$$\int_{S'} B_z(x, y) dS + \mu_0 \Lambda \int_{C'} \mathbf{J} \cdot d\mathbf{l} = n\phi_0. \quad (10)$$

For the general case when the SQUID is subject to a perpendicular applied magnetic induction B_a , carries a current I unequally divided between the two arms, $I_1 = I/2 - I_d$ and $I_2 = I/2 + I_d$, where the circulating current¹⁹ is $I_d = (I_2 - I_1)/2$, and contains a vortex at the position \mathbf{r}_v in the body of the SQUID, the *effective flux* Φ in the z direction can be written as the sum of four independent contributions:

$$\Phi = \Phi_I + \Phi_d + \Phi_f + \Phi_v, \quad (11)$$

The first term on the right-hand side of Eq. (11) is that which would be produced by equal currents $I/2$ in the y direction on the left and right sides of the SQUID shown in Fig. 1:

$$\Phi_I = \int_S B_I(x, y) dS + \mu_0 \Lambda \int_C \mathbf{J}_I \cdot d\mathbf{l}, \quad (12)$$

where $B_I(x, y)$ is the z component of the self-field generated via the Biot-Savart law by the sheet-current density $\mathbf{J}_I(x, y)$, subject to the condition that the same current $I/2$ flows through the two contacts a and b . For a symmetric SQUID, $J_I(x, y)$, the y component of $\mathbf{J}_I(x, y)$, is then an even function of x , and $J_I(x, y)$ and $B_I(x, y)$ are odd functions of x . As a result, both terms on the right-hand side of Eq. (12) vanish by symmetry, and $\Phi_I = 0$. Since $\nabla \cdot \mathbf{J}_I = 0$ except at the contacts a and b , we may write $\mathbf{J}_I = -(I/2)\nabla \times \mathbf{G}_I$, where $\mathbf{G}_I = \hat{z}G_I$, such that $\mathbf{J}_I(x, y) = (I/2)\hat{z} \times \nabla G_I(x, y)$. The contours of the scalar stream function $G_I(x, y) = \text{const}$ correspond to streamlines of $\mathbf{J}_I(x, y)$, and we may choose $G_I = 0$ for points $\mathbf{r}_i = (x_i, y_i)$ all along the inner edges of the superconductors and $G_I = 1$ for points $\mathbf{r}_o = (x_o, y_o)$ all along the outer right edges and $G_I = -1$ for points $\mathbf{r}_o = (x_o, y_o)$ all along the outer left edges.

The second term on the right-hand side of Eq. (11) is due to the circulating current¹⁹ $I_d = (I_2 - I_1)/2$ in the counterclockwise direction when unequal currents flow in the two sides of the SQUID shown in Fig. 1:

$$\Phi_d = \int_S B_d(x, y) dS + \mu_0 \Lambda \int_C \mathbf{J}_d \cdot d\mathbf{l}, \quad (13)$$

where $B_d(x, y)$ is the z component of the self-field generated via the Biot-Savart law by the circulating sheet-current density $\mathbf{J}_d(x, y)$ when a current I_d flows through

contact a from the counterelectrode into the body of the SQUID, passes around the central hole, and flows through contact b back into the counterelectrode. The magnetic moment m_d generated by the circulating current is proportional to I_d , as can be seen from Eq. (7). Since $\nabla \cdot \mathbf{J}_d = 0$ except at the contacts a and b , we may write $\mathbf{J}_d = -I_d \nabla \times \mathbf{G}_d$, where $\mathbf{G}_d = \hat{z}G_d$, such that $\mathbf{J}_d(x, y) = I_d \hat{z} \times \nabla G_d(x, y)$. The contours of the scalar stream function $G_d(x, y) = \text{const}$ correspond to streamlines of $\mathbf{J}_d(x, y)$, and we may choose $G_d = 0$ for points $\mathbf{r}_i = (x_i, y_i)$ all along the inner edges of the superconductors and $G_d = 1$ for points $\mathbf{r}_o = (x_o, y_o)$ all along the outer edges. Once a numerical result for Φ_d is found, the result can be used to determine the inductance L of the SQUID via $L = \Phi_d/I_d$, as was done for a circular ring in Ref. 31. The resulting expression for L is the sum of the geometric and kinetic inductances.

The third term on the right-hand side is a *flux-focusing* term due to the applied field:

$$\Phi_f = \int_S B_f(x, y) dS + \mu_0 \Lambda \int_C \mathbf{J}_f \cdot d\mathbf{l}, \quad (14)$$

where $B_f(x, y)$ is the z component of the net magnetic induction in the plane of the SQUID produced by the sum of a perpendicular applied field B_a and the z component of the self-field $B_{sf}(x, y)$ generated via the Biot-Savart law by the sheet-current density $\mathbf{J}_f(x, y)$ induced in response to B_a , subject to the condition that no current flows through the junctions a and b . In other words, the desired fields are those that would appear in response to B_a if the junctions a and b were open-circuited. Since $\nabla \cdot \mathbf{J}_f = 0$, we may write $\mathbf{J}_f = -\nabla \times \mathbf{G}_f$, where $\mathbf{G}_f = \hat{z}G_f$, such that $\mathbf{J}_f(x, y) = \hat{z} \times \nabla G_f(x, y)$. The contours of the scalar stream function $G_f(x, y) = \text{const}$ correspond to streamlines of $\mathbf{J}_f(x, y)$, and we may choose $G_f = 0$ for all points (x, y) along the inner and outer edges of the superconductor. Once a numerical result for Φ_f is found, the result can be used to determine the effective area²⁰ of the SQUID's central hole, $A_{\text{eff}} = \Phi_f/B_a$, as was done for a circular ring in Ref. 31.

To prove that the effective area is also given by $A_{\text{eff}} = m_d/I_d$,³² we consider the electromagnetic energy cross term $E_{fd} = \int (\mathbf{B}_f \cdot \mathbf{B}_d/\mu_0 + \mu_0 \lambda^2 \mathbf{j}_f \cdot \mathbf{j}_d) d^3r$, where the integral extends over all space. Here, $\mathbf{B}_f(\mathbf{r}) = \mathbf{B}_a(\mathbf{r}) + \mathbf{B}_{sf}(\mathbf{r}) = \nabla \times \mathbf{A}_f(\mathbf{r})$, where $\mathbf{j}_a(\mathbf{r}) = \nabla \times \mathbf{B}_a(\mathbf{r})/\mu_0$ is the current density in the distant coil that produces a nearly uniform field B_a in the vicinity of the SQUID, $\mathbf{j}_f = \nabla \times \mathbf{B}_{sf}/\mu_0$ is the induced current density in the SQUID, and \mathbf{B}_{sf} is the corresponding self-field under the conditions of flux focusing, i.e., when $\mathbf{j}_f = 0$ through the junctions. Also, $\mathbf{B}_d = \nabla \times \mathbf{A}_d$ is the dipole-like field distribution generated by the circulating current I_d with density \mathbf{j}_d in the SQUID; at large distances from the SQUID²³ $\mathbf{A}_d = \mu_0 \mathbf{m}_d \times \mathbf{r}/4\pi r^3$. We evaluate E_{fd} in two ways, making use of the vector identities $\nabla \cdot (\mathbf{A} \times \mathbf{B}) = \mathbf{B} \cdot (\nabla \times \mathbf{A}) - \mathbf{A} \cdot (\nabla \times \mathbf{B})$ and $\nabla \cdot (\gamma \mathbf{j}) = \gamma \nabla \cdot \mathbf{j} + \nabla \gamma \cdot \mathbf{j}$, and applying the divergence theorem, first with $\mathbf{A} = \mathbf{A}_d$, $\mathbf{B} = \mathbf{B}_f$, $\gamma = \gamma_d$, and $\mathbf{j} = \mathbf{j}_f$, from which we obtain

$E_{fd} = B_a m_d$, and then with $\mathbf{A} = \mathbf{A}_f$, $\mathbf{B} = \mathbf{B}_d$, $\gamma = \gamma_f$, and $\mathbf{j} = \mathbf{j}_d$, from which we obtain $E_{fd} = \Phi_f I_d$ with the help of Eq. (3). Since $\Phi_f = B_a A_{\text{eff}}$, the effective area obeys $A_{\text{eff}} = m_d/I_d$.

The fourth term on the right-hand side of Eq. (11) is due to a vortex at position $\mathbf{r}_v = \hat{x}x_v + \hat{y}y_v$ in the body of the SQUID:

$$\Phi_v(\mathbf{r}_v) = \int_S B_v(x, y) dS + \mu_0 \Lambda \int_C \mathbf{J}_v \cdot d\mathbf{l}, \quad (15)$$

where $B_v(x, y)$ is the z component of the self-field generated by the vortex's sheet-current density $\mathbf{J}_v(x, y)$ via the Biot-Savart law when no current flows through the junctions a and b . The desired fields are those that would appear in response to the vortex if the junctions a and b were open-circuited. Since $\nabla \cdot \mathbf{J}_v = 0$, it is possible to express $\mathbf{J}_v(x, y)$ in terms of a scalar stream function, as we did for $\mathbf{J}_f(x, y)$ and $\mathbf{J}_d(x, y)$. However, as shown below, it is possible to use energy arguments to express $\Phi_v(x, y)$ in terms of the stream function $G_d(x, y)$.³³

To obtain $\Phi_v(\mathbf{r})$ when a vortex is at the position $\mathbf{r} = \hat{x}x + \hat{y}y$, imagine disconnecting the counterelectrode in Fig. 1 and attaching leads from a power supply to the contacts a and b . The power supply provides a constant current I_d in the counterclockwise direction, and the sheet-current distribution through the body of the SQUID is given by $\mathbf{J}_d(x, y) = I_d \hat{z} \times \nabla G_d(x, y)$, as discussed above. We also imagine attaching leads from a high-impedance voltmeter to the contacts a and b . If the vortex moves, the effective flux Φ_v changes with time, and the voltage read by the voltmeter will be³⁴ $V_{ab} = d\Phi_v/dt$. The power delivered by the power supply can be expressed in terms of the Lorentz force on the vortex, $\mathbf{J}_d \times \hat{z}\phi_0 = I_d \phi_0 \nabla G_d$; i.e., the rate at which work is done on the moving vortex is $I_d \phi_0 \nabla G_d \cdot d\mathbf{r}/dt$. Equating this to the power $P = I_d d\Phi_v/dt = I_d \nabla \Phi_v \cdot d\mathbf{r}/dt$ delivered by the power supply to maintain constant current, we obtain the equation $\nabla \Phi_v(\mathbf{r}) = \phi_0 \nabla G_d(\mathbf{r})$. Thus $\Phi_v(\mathbf{r}) = \phi_0 G_d(\mathbf{r}) + \text{const}$, where the constant can have one of two possible values depending upon whether the integration contour C is chosen to run inside or outside the vortex axis at $\mathbf{r} = \hat{x}x + \hat{y}y$. Choosing C to run around the outer boundary of the SQUID, we obtain

$$\Phi_v(\mathbf{r}) = \phi_0 G_d(\mathbf{r}). \quad (16)$$

Since $G_d(\mathbf{r}_o) = 1$ for points $\mathbf{r} = \mathbf{r}_o$ on the outer edges of the SQUID and $G_d(\mathbf{r}_i) = 0$ for points $\mathbf{r} = \mathbf{r}_i$ on the inner edges (at the perimeter of the central hole or along the edges of the slit), we have $\Phi_v(\mathbf{r}_o) = \phi_0$ and $\Phi_v(\mathbf{r}_i) = 0$. The derivation of Eq. (16) implicitly assumes that the vortex-core radius is much smaller than the linear dimensions of the SQUID.

We now return to the problem of how to find the currents I and I_d in the SQUID, as well as the critical current I_c . As discussed above, we have $\Phi_I = 0$ for a symmetric SQUID. For simplicity, we assume first that there are no vortices in the body of the SQUID, such that

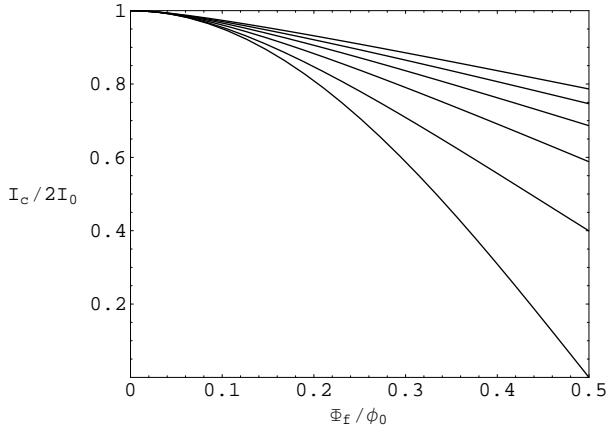


FIG. 2: $I_c/2I_0$ vs Φ_f/ϕ_0 , calculated from Eqs. (17) and (18), for $\pi LLI_0/\phi_0 = 0, 1, 2, 3, 4,$ and 5 (bottom to top).

$\Phi_v = 0$ and $\Phi = \Phi_f + \Phi_d$ in Eq. (3), where $\Phi_d = LLI_d$. From the sum and the difference of I_1 and I_2 we obtain

$$I = 2I_0 \cos\left(\frac{\pi\Phi_f}{\phi_0} + \frac{\pi LLI_d}{\phi_0}\right) \sin \bar{\phi}, \quad (17)$$

$$I_d = -I_0 \sin\left(\frac{\pi\Phi_f}{\phi_0} + \frac{\pi LLI_d}{\phi_0}\right) \cos \bar{\phi}, \quad (18)$$

where $\bar{\phi} = (\phi_1 + \phi_2)/2$ is determined experimentally by how much current is applied to the SQUID. When $\bar{\phi} = 0$, the current I is zero. As $\bar{\phi}$ increases, the magnitude of I increases and reaches its maximum value I_c at a value of $\bar{\phi}$ that must be determined by numerically solving Eqs. (17) and (18). A simple solution is obtained for arbitrary Φ_f only in the limit $\pi LLI_0/\phi_0 \rightarrow 0$, for which $I = I_c = 2I_0 |\cos(\pi\Phi_f/\phi_0)|$ and $I_d = 0$ at the critical current. For values of $\pi LLI_0/\phi_0$ of order unity, as is the case for practical SQUIDs, one may obtain I_c for any value of Φ_f by solving Eq. (18) self-consistently for I_d for a series of values of $\bar{\phi}$ and by substituting the results into Eq. (17) to determine which value of $\bar{\phi}$ maximizes I . Equations (17) and (18) have been solved numerically by de Bruyn Ouboter and de Waele,²⁴ (some of their results are also shown by Orlando and Delin²¹), who showed that at I_c

$$I_c(\Phi_f) = I_c(\Phi_f + n\phi_0) = I_c(-\Phi_f), \quad (19)$$

$$I_d(\Phi_f) = I_d(\Phi_f + n\phi_0) = -I_d(-\Phi_f), \quad (20)$$

$$I_1(\Phi_f) = I_1(\Phi_f + n\phi_0) = I_2(-\Phi_f), \quad (21)$$

$$I_2(\Phi_f) = I_2(\Phi_f + n\phi_0) = I_1(-\Phi_f), \quad (22)$$

where n is an integer. Hence all the physics is revealed by displaying $I_c(\Phi_f)$ over the interval $0 \leq \Phi_f \leq \phi_0/2$, as shown in Fig. 2.

When a vortex is present, Eqs. (17) and (18) still hold, except that Φ_f in these equations is replaced by the sum $\Phi_f + \Phi_v$. Thermally agitated motion of vortices in the body of the SQUID can produce flux noise via the term $\Phi_v(\mathbf{r}_v)$ and the time dependence of the vortex position

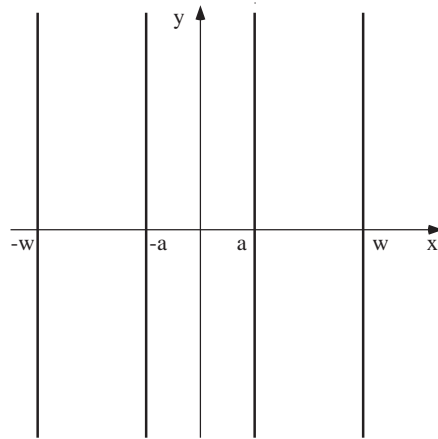


FIG. 3: Sketch of central portion of the long SQUID considered in Sec. III.

\mathbf{r}_v . From Eq. (16) we see that the sensitivity of I_c to vortex-position noise is proportional to the magnitude of $\nabla\Phi_v(\mathbf{r}) = \phi_0\nabla G_d = \mathbf{J}_d \times \hat{z}\phi_0/I_d$. Thus I_c is most sensitive to vortex-position noise when the vortices are close to the inner or outer edges of the SQUID, where the magnitude of \mathbf{J}_d is largest. These equations provide more accurate results for the vortex-position sensitivity than the approximations given in Refs. 2 and 35.

So far, we have investigated how the general equations governing the behavior of a dc SQUID are altered when the contributions arising from line integrals of the current density are included. As we have shown in Ref. 31, these additional contributions are important when the Pearl length Λ is an appreciable fraction of the linear dimensions of the SQUID. We have found that the basic SQUID equations, Eqs. (17) and (18), are unaltered, except that the magnetic flux (sometimes called Φ_{ext} ²¹) generated in the SQUID's central hole by the externally applied field in the absence of a vortex is replaced by the *effective flux* Φ_f , given in Eq. (14). Similarly, we have shown that the total inductance L of the SQUID has contributions both from the magnetic induction (geometric inductance) and the associated supercurrent (kinetic inductance). We also have shown in principle how to calculate the effect of the return flux from a vortex at position \mathbf{r}_v in the body of the SQUID, and we have found that the effective flux arising from the vortex is $\Phi_v(\mathbf{r}_v)$, given in Eqs. (15) and (16). To demonstrate that all the above quantities can be calculated numerically for arbitrary values of Λ , we next examine the behavior of a model SQUID as described in Sec. III.

III. LONG SQUID IN A PERPENDICULAR MAGNETIC FIELD

Here we consider a long SQUID whose thickness d is less than the London penetration depth λ and whose topology is like that of Fig. 1 but which is stretched

to a large length l in the y direction, as sketched in Fig. 3. SQUIDS of similar geometry have been investigated experimentally in Refs. 14,36,37,38,39. We treat here the case for which the length l is much larger than the width $2w$ of the body of the SQUID, and we focus on the current and field distributions in and near the left ($-w < x < -a$) and right ($a < x < w$) arms and near the center of the SQUID, where to a good approximation the current density j_y is uniform across the thickness and depends only upon x , and the magnetic induction $\mathbf{B} = \nabla \times \mathbf{A}$ depends only upon x and z . In the equations that follow, we deal with the sheet-current density, whose component in the y direction is $J_y(x) = j_y(x)d$.

The self-field magnetic induction generated by $J_y(x)$ is $\mathbf{B}_J(x, z) = \nabla \times \mathbf{A}_J(x, z)$, where $A_J(x, z)$, the y component of the vector potential obtained from Ampere's law, is

$$A_J(x, z) = \frac{\mu_0}{2\pi} \int J_y(x') \ln \frac{C}{\sqrt{(x-x')^2 + z^2}} dx'. \quad (23)$$

The integration here and in the following equations is carried out only over the strips, and C is a constant with dimensions of length remaining to be determined. In the presence of a perpendicular applied field $\mathbf{B}_a = \hat{z}B_a = \nabla \times \mathbf{A}_f$, the total vector potential is $\mathbf{A} = \mathbf{A}_J + \mathbf{A}_f$, where $\mathbf{A}_f = \hat{y}B_ax$.

A. Formal solutions

We now use the approach of Ref. 40 to calculate the in-plane magnetic-induction and sheet-current distributions appearing in Eqs. (11)-(14) in Sec. II. For all of these contributions we shall take into account the in-plane ($z = 0$) self-field contribution $A_J(x) = A_J(x, 0)$ to the y component of the vector potential, where

$$A_J(x) = \frac{\mu_0}{2\pi} \int J_y(x') \ln \frac{C}{|x-x'|} dx'. \quad (24)$$

We first examine the *equal-current case* and consider the contributions $B_I(x)$, the z component of $\mathbf{B}_I(x)$, and $J_I(x)$, the y component of $\mathbf{J}_I(x)$, due to equal currents $I/2$ in the left and right sides of the SQUID. Since $J_I(-x) = J_I(x)$, the corresponding y component of the vector potential is also a symmetric function of x : $A_I(-x) = A_I(x)$, where the subscripts I refer to the equal-current case. There are no flux quanta between the strips ($\Phi_I = 0$), and the second term in the brackets on the right-hand side of Eq. (1) vanishes; $(\phi_0/2\pi)\nabla\gamma = 0$. However, the constant C must be chosen such that $J_I(x) = -A_I(x)/\mu_0\Lambda$ in the superconductor. Combining this equation with Eq. (24), making use of the symmetry $J_I(-x) = J_I(x)$, and noting that $I = 2 \int_a^w J_I(x)dx$, we obtain

$$\frac{I}{2\pi} \ln \frac{b}{C} = \int_a^w \left[\frac{1}{2\pi} \ln \frac{b^2}{|x^2-x'^2|} + \Lambda\delta(x-x') \right] J_I(x') dx' \quad (25)$$

for $a < x < w$. Here b can be chosen to be any convenient length, such as the length l or w , but not C . We now define the inverse integral kernel $K^{\text{sy}}(x, x')$ for the symmetric-current case via

$$\int_a^w K^{\text{sy}}(x, x'') \left[\frac{1}{2\pi} \ln \frac{b^2}{|x''^2-x'^2|} + \Lambda\delta(x''-x') \right] dx'' = \delta(x-x'). \quad (26)$$

Applying this kernel to Eq. (25), we obtain

$$J_I(x) = \frac{I}{2\pi} \ln \left(\frac{b}{C} \right) \int_a^w K^{\text{sy}}(x, x') dx'. \quad (27)$$

Since $I = 2 \int_a^w J_I(x)dx$, we find

$$\ln \left(\frac{b}{C} \right) = \pi / \int_a^w \int_a^w K^{\text{sy}}(x, x') dx dx', \quad (28)$$

such that

$$J_I(x) = \frac{I}{2} \int_a^w K^{\text{sy}}(x, x') dx' / \int_a^w \int_a^w K^{\text{sy}}(x', x'') dx' dx''. \quad (29)$$

For $a \leq x \leq w$, the stream function is

$$G_I(x) = \frac{2}{I} \int_a^x J_I(x') dx', \quad (30)$$

and for $-w \leq x \leq -a$, $G_I(-x) = -G_I(x)$. The corresponding z component of the magnetic induction $B_I(x)$ can be obtained from the Biot-Savart law or, since $B_I(x) = dA_I(x)/dx$, from Eq. (24). Note that $B_I(-x) = -B_I(x)$. Although the kernel $K^{\text{sy}}(x, x')$ depends upon b , we find numerically that $J_I(x)$ and $B_I(x)$ are independent of b .

We next examine the *circulating-current case* and consider the contributions $B_d(x)$, the z component of $\mathbf{B}_d(x)$, and $J_d(x)$, the y component of $\mathbf{J}_d(x)$, due to a circulating current I_d ; the current in the y direction on the right side of the SQUID is $I_2 = I_d$ and that on the left side is $I_1 = -I_d$. The vector potential is still given by Eq. (24), except that we add subscripts d . However, since $J_d(-x) = -J_d(x)$, the vector potential is now an anti-symmetric function of x ; $A_d(-x) = -A_d(x)$. The circulating current is generated by the fluxoid Φ_d [see Eq. (13)] associated with a nonvanishing gradient of the phase γ around the loop. The second term inside the bracket on the right-hand side of Eq. (1), $(\phi_0/2\pi)\nabla\gamma$, is $-\hat{y}\Phi_d/2l$ for $a < x < w$ and $\hat{y}\Phi_d/2l$ for $-w < x < -a$. Thus, $J_d(x) = -[A_d(x) - \Phi_d/2l]/\mu_0\Lambda$ for $a < x < w$. Combining this equation with that for $A_d(x)$, noting that the inductance of the SQUID is $L = \Phi_d/I_d$, and making use of the symmetry $J_d(-x) = -J_d(x)$, we obtain

$$\frac{LI_d}{2l} = \mu_0 \int_a^w \left[\frac{1}{2\pi} \ln \left| \frac{x+x'}{x-x'} \right| + \Lambda\delta(x-x') \right] J_d(x') dx' \quad (31)$$

for $a < x < w$. We now define the inverse integral kernel $K^{\text{as}}(x, x')$ for the asymmetric-current case via

$$\int_a^w K^{\text{as}}(x, x'') \left[\frac{1}{2\pi} \ln \left| \frac{x''+x'}{x''-x'} \right| + \Lambda\delta(x''-x') \right] dx'' = \delta(x-x'). \quad (32)$$

Applying this kernel to Eq. (31) and noting that $I_d = \int_a^w J_d(x)dx$, we obtain

$$J_d(x) = \alpha I_d \int_a^w K^{\text{as}}(x, x') dx' \quad (33)$$

and

$$L = 2\alpha\mu_0 l, \quad (34)$$

where

$$\alpha = 1 / \int_a^w \int_a^w K^{\text{as}}(x, x') dx dx' \quad (35)$$

is a dimensionless function of a, b, w , and Λ , which we calculate numerically in the next section. For $a \leq x \leq w$, the stream function is

$$G_d(x) = \frac{1}{I_d} \int_a^x J_d(x') dx', \quad (36)$$

and for $-w \leq x \leq -a$, $G_d(-x) = G_d(x)$.

In this formulation, as in Ref. 31, $L = L_m + L_k$ is the total inductance. The geometric inductance contribution $L_m = 2E_m/I_d^2$, where $E_m = l \int_a^w J_d(x) A_d(x) dx$ is the stored magnetic energy, and the kinetic contribution $L_k = 2E_k/I_d^2$, where $E_k = \mu_0 \Lambda l \int_a^w J_d^2(x) dx$ is the kinetic energy of the supercurrent, can be calculated using Eq. (33) from^{31,44,45}

$$L_m = \frac{\mu_0 l}{\pi I_d^2} \int_a^w \int_a^w \ln \left| \frac{x+x'}{x-x'} \right| J_d(x) J_d(x') dx dx', \quad (37)$$

$$L_k = \frac{2\mu_0 l \Lambda}{I_d^2} \int_a^w J_d^2(x) dx = \frac{2\mu_0 l \Lambda}{(w-a)} \frac{\langle J_d^2 \rangle}{\langle J_d \rangle^2}, \quad (38)$$

where the brackets ($\langle \rangle$) denote averages over the film width. We can show that $L_m + L_k = L$ with the help of Eqs. (32) and (35).

The z component of the magnetic induction $B_d(x)$ generated by $J_d(x)$ can be obtained from the Biot-Savart law, or, since $B_d(x) = dA_d(x)/dx$, from Eq. (24). Note that $B_d(-x) = B_d(x)$.

When $l \gg w$, the magnetic moment in the z direction generated by the circulating current I_d is (to lowest order in w/l)

$$m_d = 2l \int_a^w x J_d(x) dx, \quad (39)$$

where the factor 2 accounts for the fact⁴¹ that the currents along the y direction and those along the x direction at the ends (U-turn) give exactly the same contribution to m_d , even in the limit $l \rightarrow \infty$. To next higher order in w/l one has to replace l in Eq. (39) by $l - (w-a)q$, where $(w-a)q/2$ is the distance of the center of gravity of the x -component of the currents near each end from this end. For a single strip of width $w-a$, one has, e.g., $q = 1/3$ for

the Bean critical state (with rectangular current stream lines) and $q = 0.47$ for ideal screening ($\Lambda \ll w$).⁴²

We next examine *flux focusing*. As discussed in Sec. II, to calculate the effective area of the slot, we need to calculate the fields produced in response to a perpendicular applied magnetic induction B_a , subject to the condition that no current flows through either junction. Since this is equivalent to having both junctions open-circuited, the problem reduces to finding the fields produced in the vicinity of a pair of long superconducting strips connected by a superconducting link at only one end, i.e., when the slot of width $2a$ between the two strips is *open* at one end. However, the desired fields may be regarded as the superposition of the solutions of two separate problems when the slot has *closed* ends: (a) the fields generated in response to B_a , when $\Phi = 0$ (the *zero-fluxoid case*) and a clockwise screening current flows around the slot [second term on the right-hand side of Eq. (41) below], and (b) the fields generated in the absence of B_a , when flux quanta in the amount of Φ_f are in the slot and a counterclockwise screening current flows around the slot [first term on the right-hand side of Eq. (41)]. The desired flux-focusing solution is obtained by setting the net circulating current equal to zero.

The equations describing the fields in the flux-focusing case are derived as follows. The z component of the net magnetic induction $B_f(x)$ is the sum of B_a and the self-field $B_{\text{sf}}(x)$ generated by $J_f(x)$. The vector potential $A_y(x)$ is the sum of $B_a x$, which describes the applied magnetic induction, and the self-field contribution given by Eq. (24) but with subscripts f . Since $J_f(-x) = -J_f(x)$, the vector potential is again an antisymmetric function of x ; $A_f(-x) = -A_f(x)$. The fluxoid Φ_f [see Eq. (14)] contributes a nonvanishing gradient of the phase γ around the loop, such that the second term inside the brackets on the right-hand side of Eq. (1), $(\phi_0/2\pi)\nabla\gamma$, is $-\dot{y}\Phi_f/2l$ for $a < x < w$ and $\dot{y}\Phi_f/2l$ for $-w < x < -a$. Equation (1) yields $J_f(x) = -[B_a x + A_f(x) - \Phi_f/2l]/\mu_0 \Lambda$ for $a < x < w$. Combining this equation with that for $A_f(x)$ [Eq. (24)], making use of the symmetry $J_f(-x) = -J_f(x)$, and introducing the effective area via $\Phi_f = B_a A_{\text{eff}}$ [see Sec. II], we obtain

$$B_a (A_{\text{eff}} - 2lx)/2l = \mu_0 \int_a^w \left[\frac{1}{2\pi} \ln \left| \frac{x+x'}{x-x'} \right| + \Lambda \delta(x-x') \right] J_f(x') dx' \quad (40)$$

for $a < x < w$. We again use the inverse integral kernel $K^{\text{as}}(x, x')$ for the asymmetric-current case [Eq. (32)] to obtain

$$J_f(x) = \frac{B_a}{\mu_0} \int_a^w \left(\frac{A_{\text{eff}}}{2l} - x' \right) K^{\text{as}}(x, x') dx'. \quad (41)$$

The effective area of the SQUID A_{eff} is found from the condition that the net current around the loop is zero [$\int_a^w J_f(x) dx = 0$], which yields

$$A_{\text{eff}} = 2\alpha l \int_a^w \int_a^w x' K^{\text{as}}(x, x') dx dx'. \quad (42)$$

For $a \leq x \leq w$, the stream function is

$$G_f(x) = \int_a^x J_f(x') dx', \quad (43)$$

and for $-w \leq x \leq -a$, $G_f(-x) = G_f(x)$. The spatial distribution of the resulting z component of the in-plane magnetic induction is given by $B_f(x) = B_a + B_{sf}(x)$, where $B_{sf}(x)$ can be obtained from the Biot-Savart law or by substituting $J_f(x)$ into Eq. (24) and making use of $B_{sf}(x) = dA_f(x)/dx$. Note that $B_f(-x) = B_f(x)$. The resulting magnetic moment m_f in the z direction can be calculated by replacing J_d by J_f in Eq. (39).

In the next section we also present numerical results for field and current distributions in the *zero-fluxoid case*, in which $I = 0$, $\Phi_v = 0$, and the effective flux is zero: $\Phi = \Phi_d + \Phi_f = 0$. Such a case could be achieved by short-circuiting the Josephson junctions in Fig. 1, cooling the device in zero field such that initially $\Phi = 0$, and then applying a small perpendicular magnetic induction B_a . A circulating current $J(x)$, given by the second term on the right-hand side of Eq. (41), would spontaneously arise in order to keep $\Phi = 0$, as in the Meissner state.

B. Numerical solutions

In the previous section we have presented formal solutions for the sheet-current density $J_y(x)$ in Eqs. (29), (33), and (41), which are expressed as integrals involving the geometry-dependent inverse kernels $K^{sy}(x, x')$ and $K^{as}(x, x')$. As in Ref. 31 for thin rings, these integrals are evaluated on a grid x_i ($i = 1, 2, \dots, N$) spanning only the strip (but avoiding the edges, where the integrand may have infinities), $a < |x_i| < w$, such that for any function $f(x)$ one has $\int_a^w f(x) dx = \sum_{i=1}^N w_i f(x_i)$. Here w_i are the weights, approximately equal to the local spacing of the x_i ; the weights obey $\sum_{i=1}^N w_i = w - a$. We have chosen the grid such that the weights w_i are narrower and the grid points x_i more closely spaced near the edges a and w , where $J_y(x)$ varies more rapidly. We have accomplished this by choosing some appropriate continuous function $x(u)$ and an auxiliary discrete variable $u_i \propto i - \frac{1}{2}$, such that $w_i = x'(u_i)(u_2 - u_1)$. We can choose $x(u)$ such that its derivative $x'(u)$ vanishes (or is reduced) at the strip edges to give a denser grid there. By choosing an appropriate substitution function $x(u)$ one can make the numerical error of this integration method arbitrarily small, decreasing rapidly with any desired negative power of the grid number N , e.g., N^{-2} or N^{-3} .

For the *equal-current case*, Eq. (25) becomes

$$\frac{I}{2\pi} \ln \frac{b}{C} = \sum_{j=1}^N (w_j Q_{ij}^{sy} + \Lambda \delta_{ij}) J_I(x_j) \quad (44)$$

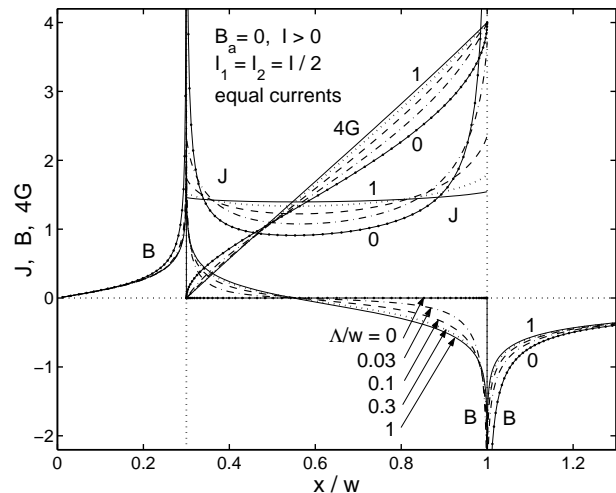


FIG. 4: Profiles of the sheet current $J_I(x)$, Eq. (49), stream function $G_I(x)$, Eq. (50), and magnetic induction $B_I(x)$ for the *equal-current case* ($B_a = 0$, $I_1 = I_2 = I/2 > 0$). Shown are the examples $a/w = 0.3$ with $\Lambda/w = 0$ (solid lines with dots), 0.03 (dot-dashed lines), 0.1 (dashed lines), 0.3 (dotted lines), and 1 (solid lines). Here B/μ_0 and J are in units I_2/w and G in units I_2 .

where $\delta_{ij} = 0$ for $i \neq j$, $\delta_{ii} = 1$, and

$$Q_{ij}^{sy} = \frac{1}{2\pi} \ln \frac{b^2}{|x_i^2 - x_j^2|}, \quad i \neq j, \\ Q_{ii}^{sy} = \frac{1}{2\pi} \ln \frac{\pi b^2}{x_i w_i}. \quad (45)$$

The optimum choice of the diagonal term Q_{ii}^{sy} (i.e., with $|x_i^2 - x_j^2|$ replaced by $x_i w_i / \pi$ for $i = j$, which reduces the numerical error from order N^{-1} to N^{-2} or higher depending on the grid) is discussed in Eq. (3.12) of Ref. 41 for strips and in Eq. (18) of Ref. 31 for disks and rings. The superscript (sy) is a reminder that this is for a symmetric current distribution [$J_I(-x) = J_I(x)$]. Defining $K_{ij}^{sy} = (w_j Q_{ij}^{sy} + \Lambda \delta_{ij})^{-1}$, such that

$$\sum_{k=1}^N K_{ik}^{sy} (w_j Q_{kj}^{sy} + \Lambda \delta_{kj}) = \delta_{ij}, \quad (46)$$

and applying it to Eq. (44), we obtain

$$J_I(x_i) = \frac{I}{2\pi} \ln \left(\frac{b}{C} \right) \sum_{j=1}^N K_{ij}^{sy}. \quad (47)$$

Since $I = 2 \sum_{i=1}^N w_i J_I(x_i)$, we find

$$\ln \left(\frac{b}{C} \right) = \pi / \sum_{i=1}^N \sum_{j=1}^N w_i K_{ij}^{sy}, \quad (48)$$

such that

$$J_I(x_i) = \frac{I}{2} \sum_{j=1}^N K_{ij}^{sy} / \sum_{k=1}^N \sum_{l=1}^N w_k K_{kl}^{sy}. \quad (49)$$

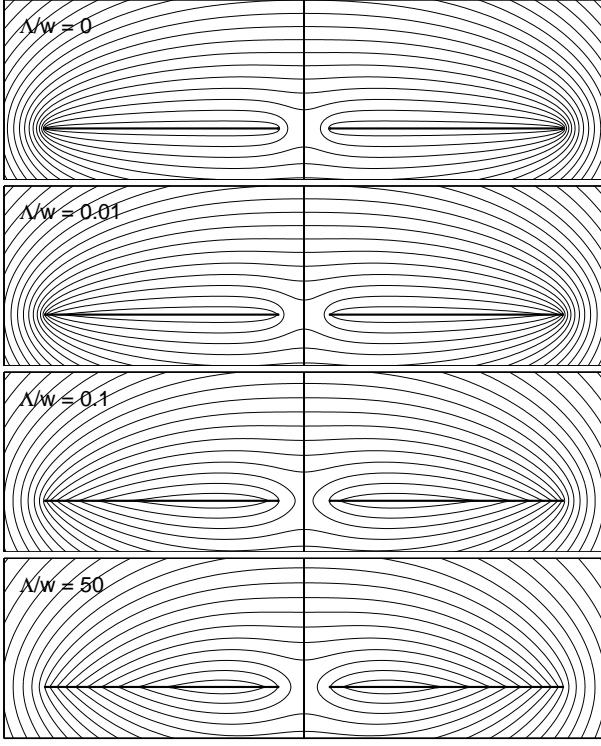


FIG. 5: Magnetic field lines in the *equal-current case* for $a/w = 0.1$ and $\Lambda/w = 0, 0.01, 0.1,$ and 50 (or ∞).

It is remarkable that although the parameter b appears in Eq. (45), the final result for $J_I(x_i)$ in Eq. (49) does not depend upon b . The stream function $G_I(x)$ can be evaluated as⁴³

$$G_I(x_i) = \sum_{j=1}^i \sum_{k=1}^N w_j K_{jk}^{\text{sy}} / \sum_{l=1}^N \sum_{m=1}^N w_l K_{lm}^{\text{sy}}. \quad (50)$$

Shown in Fig. 4 are plots of $J_I(x)$, $G_I(x)$, and the corresponding magnetic induction $B_I(x)$ vs x for $a/w = 0.3$ and various values of $\Lambda/w = 0, 0.03, 0.1, 0.3, 1$. The curves for $\Lambda = 0$ exactly coincide with the analytic expressions of Appendix A. The magnetic field lines for this case are depicted in Fig. 5.

For the *circulating-current case*, Eq. (31) becomes

$$\frac{L I_d}{2l} = \mu_0 \sum_{j=1}^N (w_j Q_{ij}^{\text{as}} + \Lambda \delta_{ij}) J_d(x_j) \quad (51)$$

where

$$\begin{aligned} Q_{ij}^{\text{as}} &= \frac{1}{2\pi} \ln \frac{x_i + x_j}{|x_i - x_j|}, \quad i \neq j, \\ Q_{ii}^{\text{as}} &= \frac{1}{2\pi} \ln \frac{4\pi x_i}{w_i}, \end{aligned} \quad (52)$$

The superscript (as) is a reminder that this is for an asymmetric current distribution [$J_d(-x) = -J_d(x)$].

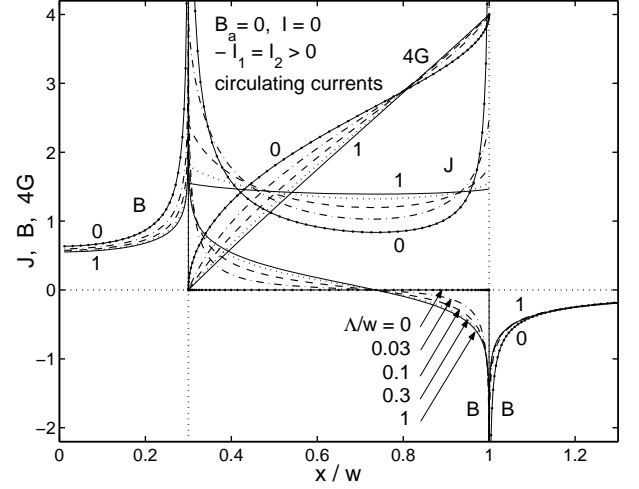


FIG. 6: Profiles of $J_d(x)$, Eq. (54), $G_d(x)$, Eq. (57), and magnetic induction $B_d(x)$ for the *circulating-current case* ($B_a = 0$, $-I_1 = I_2 > 0$). Shown are the examples $a/w = 0.3$ with $\Lambda/w = 0$ (solid lines with dots), 0.03 (dot-dashed lines), 0.1 (dashed lines), 0.3 (dotted lines), and 1 (solid lines). B/μ_0 and J are in units I_2/w and G in units I_2 .

Defining $K_{ij}^{\text{as}} = (w_j Q_{ij}^{\text{as}} + \Lambda \delta_{ij})^{-1}$, such that

$$\sum_{k=1}^N K_{ik}^{\text{as}} (w_j Q_{kj}^{\text{as}} + \Lambda \delta_{kj}) = \delta_{ij}, \quad (53)$$

applying it to Eq. (51), and noting that $I_d = \sum_{i=1}^N w_i J_d(x_i)$, we obtain

$$J_d(x_i) = \alpha I_d \sum_{j=1}^N K_{ij}^{\text{as}} \quad (54)$$

and

$$L = 2\alpha \mu_0 l, \quad (55)$$

where

$$\alpha = 1 / \sum_{i=1}^N \sum_{j=1}^N w_i K_{ij}^{\text{as}}. \quad (56)$$

The stream function $G_d(x)$ can be evaluated as⁴³

$$G_d(x_i) = \alpha \sum_{j=1}^i \sum_{k=1}^N w_j K_{jk}^{\text{sy}}. \quad (57)$$

Shown in Fig. 6 are plots of $J_d(x)$, $G_d(x)$, and $B_d(x)$ vs x for $a/w = 0.3$ and various values of Λ/w . Note that these curves look similar to those in Fig. 4, but they all have opposite parity, as can be seen from the different profiles $B(x)$ near $x = 0$. The magnetic field lines for this case are shown in Fig. 7.

As discussed in Sec. II, when a vortex is present in the region $a < |x| < w$, the sensitivity of the SQUID's

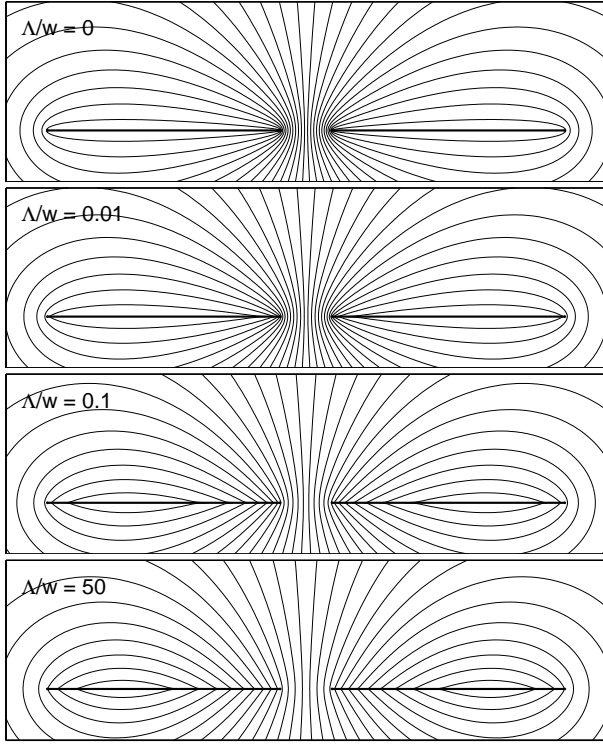


FIG. 7: Magnetic field lines in the *circulating-current* case for $a/w = 0.1$ and $\Lambda/w = 0, 0.01, 0.1,$ and 50 (or ∞).

critical current I_c is proportional to the magnitude of $d\Phi_v/dx = \phi_0 dG_d/dx = \phi_0 J_d(x)/I_d$. From Fig. 6 we see that when $\Lambda \ll w$, this sensitivity is greatly enhanced when the vortex is close to the edges a and w but that when $\Lambda \geq w$, the sensitivity is nearly independent of position.

Shown as the solid curves in Fig. 8(a) are plots of the inductance L vs a/w for various values of $\Lambda/w = 0, 0.03, 0.1, 0.3,$ and 1 . The solid curves in Fig. 9(a) show the same L vs Λ/w (range 0.0045 to 2.2) for several values of $a/w = 0.01, 0.1, 0.4, 0.8, 0.95,$ and 0.99 .

The geometric and kinetic contributions L_m and L_k can be calculated separately from Eqs. (37) and (38)

$$L_m = \frac{2\mu_0 l}{I_d^2} \sum_{i=1}^N \sum_{j=1}^N w_i w_j Q_{ij}^{\text{as}} J_d(x_i) J_d(x_j), \quad (58)$$

$$L_k = \frac{2\mu_0 l \Lambda}{I_d^2} \sum_{i=1}^N \sum_{j=1}^N w_i J_d^2(x_i), \quad (59)$$

using Eqs. (54) and (56). We can show that $L_m + L_k = L$ using the property of inverse matrices that $\mathbf{M} \cdot \mathbf{M}^{-1} = \mathbf{M}^{-1} \cdot \mathbf{M} = \mathbf{I}$, where \mathbf{I} is the identity matrix.

Shown as solid curves in Fig. 8(b) are L_m and L_k vs a/w . For $\Lambda = 0$, when $L_k = 0$, $L = L_m$ exactly coincides with Eq. (A10), which may be approximated by Eq. (A11) for $a/w < 0.7$ [open circles in Fig. 8(a)] and by Eq. (A12) for $a/w > 0.7$ [open squares in Fig. 8(a)]. The dotted curves in Fig. 8(b) for L_m and L_k are those

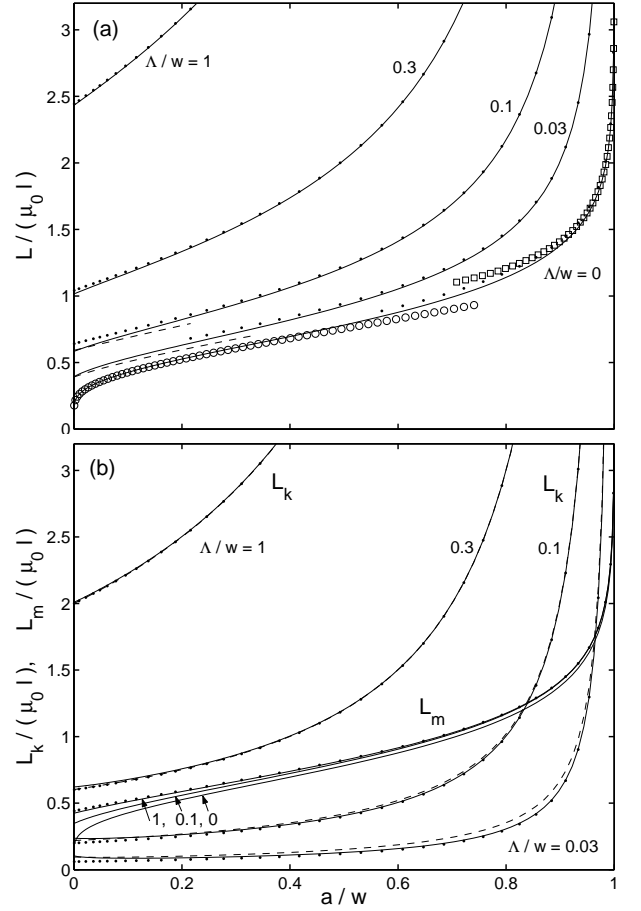


FIG. 8: (a) Solid curves show the inductance $L = L_m + L_k$ [Eq. (55)] vs a/w calculated for $\Lambda/w = 0, 0.03, 0.1, 0.3,$ and 1 . See the text for descriptions of analytic approximations shown by the open circles, open squares, dots, and dashes. (b) Solid curves show the geometric inductance L_m [Eq. (58)] vs a/w for $\Lambda/w = 0, 0.1,$ and 1 and the kinetic inductance L_k [Eq. (59)] vs a/w for $\Lambda/w = 0.03, 0.1, 0.3,$ and 1 . See the text for descriptions of analytic approximations shown by the dotted and dashed curves.

of Eqs. (C3) and (C6) in the limit $\Lambda/w \rightarrow \infty$, when the circulating current density is uniform. The dotted curves in Fig. 8(a) are obtained from $L = L_m + L_k$ using the approximations of Eqs. (C3) and (C6); they are an excellent approximation to L for $\Lambda/w \geq 0.03$ except for small values of a/w . Improved agreement for small values of Λ/w and a/w is shown by the dashed curves in Fig. 8(a), which show the approximation of Eq. (B7) for L , and in Fig. 8(b), which show the approximation of Eq. (B12) for L_k .

The solid curves in Fig. 9(b) show L_m and L_k vs Λ/w . The geometric inductance L_m depends upon Λ but only weakly, varying slowly between its $\Lambda = 0$ asymptote [Eq. (A10), horizontal dot-dashed line] and its $\Lambda = \infty$ asymptote [Eq. (C3), horizontal dotted line]. For larger values of a/w , L_m is nearly independent of Λ . On the other hand, the kinetic inductance L_m , is approxi-

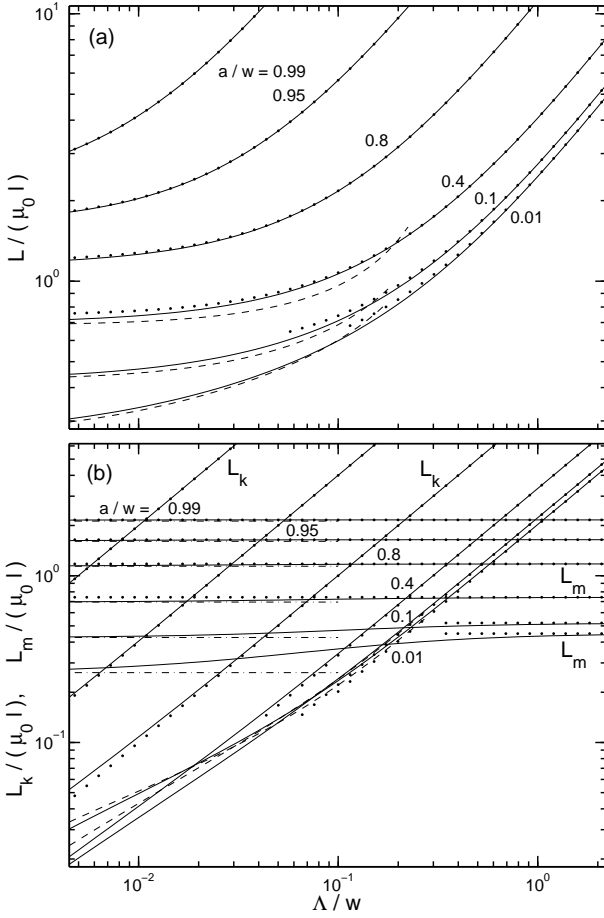


FIG. 9: (a) Solid curves show the inductance $L = L_m + L_k$ [Eq. (55)] vs Λ/w for $a/w = 0.01, 0.1, 0.4, 0.8, 0.95$, and 0.99 . See the text for descriptions of analytic approximations shown by the dotted and dashed curves. (b) Solid curves show both the geometric inductance L_m [Eq. (58)] and the kinetic inductance L_k [Eq. (59)] vs Λ/w for $a/w = 0.01, 0.1, 0.4, 0.8, 0.95$, and 0.99 . See the text for descriptions of analytic approximations shown by the dotted, dashed, and dot-dashed curves.

mately proportional to Λ/w . The straight dotted lines in Fig. 9(b), calculated from the large- Λ approximation given in Eq. (C6), are a good approximation to L_m except for small values of Λ/w and a/w . The dotted curves in Fig. 9(a) are obtained from $L = L_m + L_k$ using the approximations of Eqs. (C3) and (C6). Improved agreement for small values of Λ/w and a/w is shown by the dashed curves in Fig. 9(a), which show the approximation of Eq. (B7) for L , and in Fig. 9(b), which show the approximation of Eq. (B12) for L_k .

In Eq. (3) of Ref. 44, Yoshida et al. derived an approximate expression for the kinetic inductance when $\Lambda/w \ll 1$. We have found that their expression for L_k is not an accurate approximation to our exact numerical results. To eliminate the logarithmic divergences due to the inverse square-root dependence of the current density near the edges, Yoshida et al. followed an

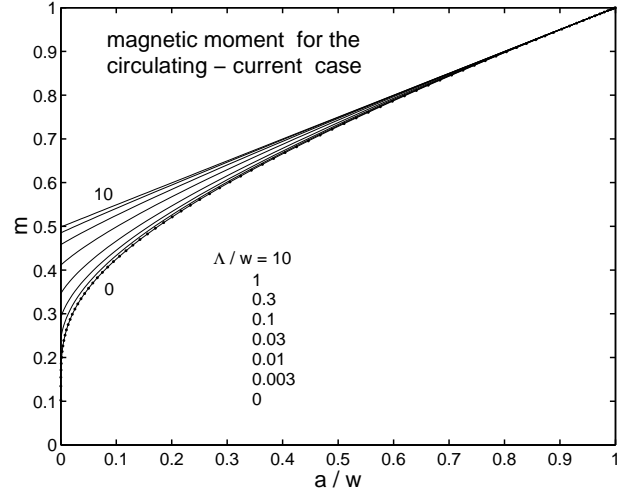


FIG. 10: The magnetic moment m_d for the *circulating current case* ($B_a = 0, -I_1 = I_2 = I_d > 0$) plotted versus a/w for various values of Λ/w in units $2wLI_d$. These curves coincide with those in Fig. 13 below.

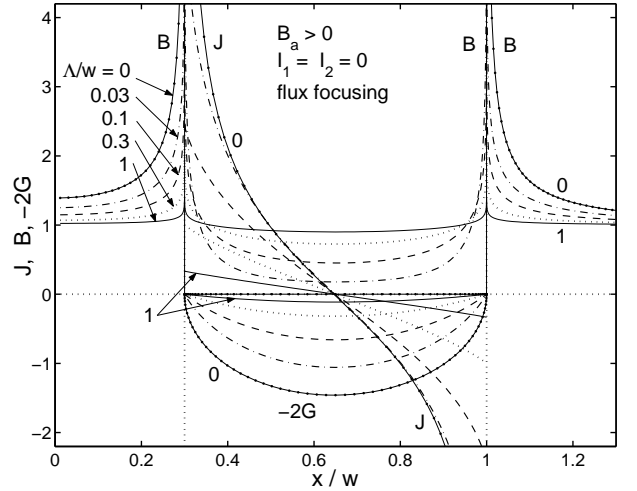


FIG. 11: Profiles $J_f(x)$, Eq. (62), $G_f(x)$, Eq. (64), and magnetic induction $B_f(x)$ for the *flux-focusing case* ($B_a > 0, I_1 = I_2 = 0$). Shown are the examples $a/w = 0.3$ with $\Lambda/w = 0$ (solid lines with dots), 0.03 (dot-dashed lines), 0.1 (dashed lines), 0.3 (dotted lines), and 1 (solid lines). B and $\mu_0 J$ are in units B_a , and G in units wB_a/μ_0 .

approach used by Meservey and Tedrow,⁴⁵ and chose a cutoff length of the order of d , the film thickness. When $d < \lambda$, however, this approach cannot be correct, because the equations describing the fields and currents in superconducting strips contain only the two-dimensional screening length $\Lambda = \lambda^2/d$. The cutoff length therefore must instead be chosen to be of the order of Λ , as we have done in Appendix B.

The magnetic moment in the z direction generated by

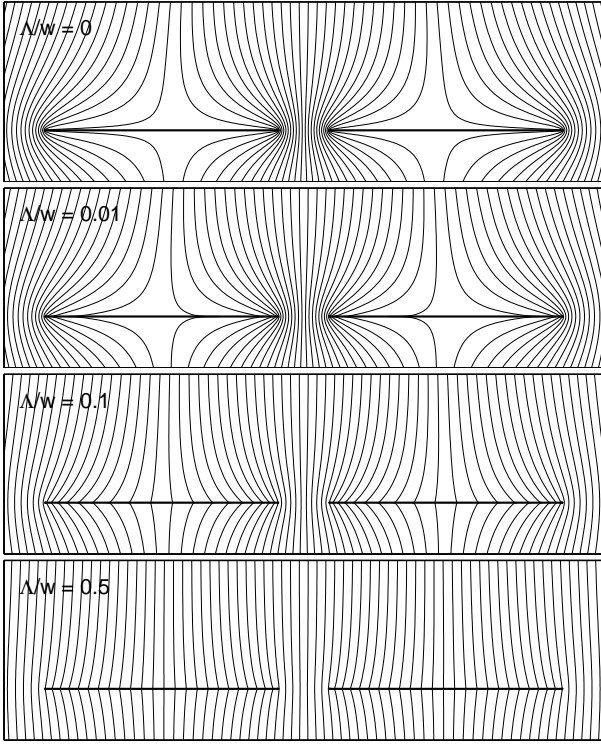


FIG. 12: Magnetic field lines in the *flux-focusing* case for $a/w = 0.1$ and $\Lambda/w = 0, 0.01, 0.1,$ and 0.5 .

the circulating current is, from Eq. (39),

$$m_d = 2 \sum_{i=1}^N w_i x_i J_d(x_i). \quad (60)$$

As shown in Fig. 10, this magnetic moment vanishes very slowly when the gap width and Λ go to zero, $a/w \rightarrow 0$ and $\Lambda/w \rightarrow 0$. This can be explained by the fact that for $\Lambda = 0$ and $a < x \ll w$ one has $J_d(x) \propto 1/x$, Eq. (A5). The contribution of these small x to m_d , Eq. (60), stays finite due to the factor x , but the total current I_d to which m_d is normalized, diverges when $a/w \rightarrow 0$, thus suppressing the plotted ratio m_d/I_d . Interestingly, the curves in Fig. 10 coincide with those in Fig. 13; see below. Expressions for m_d in the limits $\Lambda/w \rightarrow 0$ and $\Lambda/w \rightarrow \infty$ are given in Eqs. (A13) and (C7).

For the *flux-focusing* case, Eq. (40) becomes

$$B_a(A_{\text{eff}}/2l - x_i) = \mu_0 \sum_{j=1}^N (w_j Q_{ij}^{\text{as}} + \Lambda \delta_{ij}) J_f(x_j). \quad (61)$$

Applying Eq. (53), we obtain

$$J_f(x_i) = \frac{B_a}{\mu_0} \left(\frac{A_{\text{eff}}}{2l} \sum_{j=1}^N K_{ij}^{\text{as}} - \sum_{j=1}^N K_{ij}^{\text{as}} x_j \right), \quad (62)$$

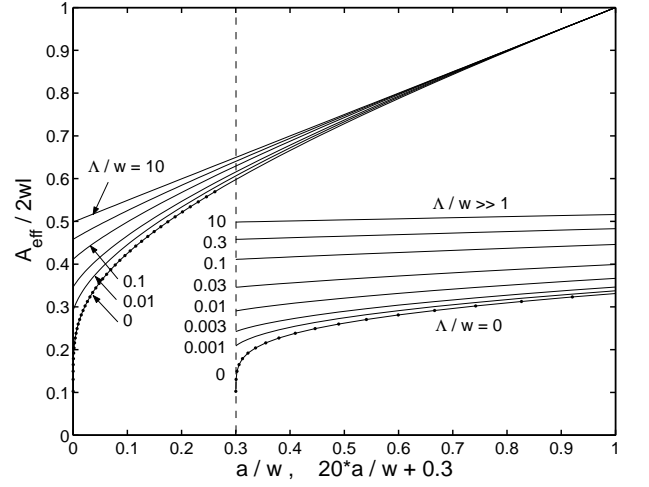


FIG. 13: The effective area A_{eff} , Eq. (63), plotted versus the gap half width a/w for several values of $\Lambda/w = 0, 0.001, 0.003, 0.01, 0.03, 0.1, 0.3,$ and 10 . The lower-right curves show the same data shifted and stretched along a/w . The dots show the exact result (A19) in the limit $\Lambda/w \rightarrow 0$. For $\Lambda/a \geq 10$ one has $A_{\text{eff}}/2wl \approx (1 + a/w)/2$, Appendix C. These curves coincide with Fig. 10 since $A_{\text{eff}} = m_d/I_d$.

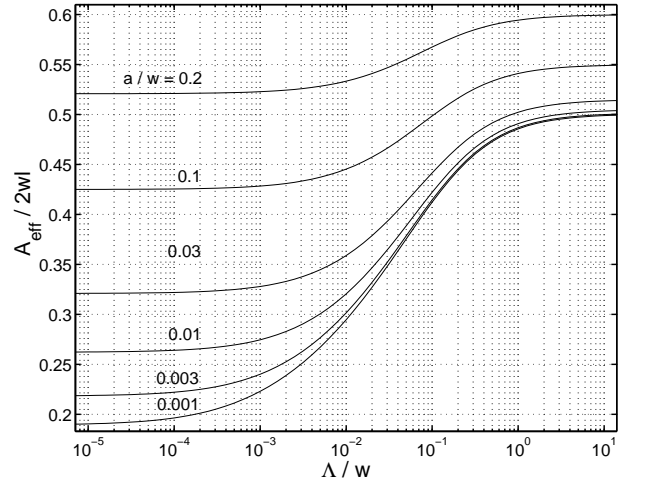


FIG. 14: The effective area A_{eff} , Eq. (63), plotted versus Λ/w (range $7 \cdot 10^{-6}$ to 14) for several values of $a/w = 0, 0.001, 0.003, 0.01, 0.03, 0.1,$ and 0.2 . Same data as in Fig. 13.

where, since $\sum_{i=1}^N w_i J_f(x_i) = 0$, the effective area is

$$A_{\text{eff}} = 2\alpha l \sum_{i=1}^N \sum_{j=1}^N w_i K_{ij}^{\text{as}} x_j. \quad (63)$$

The stream function $G_f(x)$ can be evaluated as⁴³

$$G_f(x_i) = \sum_{j=1}^i w_j J_f(x_j). \quad (64)$$

Shown in Fig. 11 are plots of the flux-focusing $J_f(x)$, $G_f(x)$, and $B_f(x)$ vs x for $a/w = 0.3$ and $\Lambda/w = 0, 0.03,$

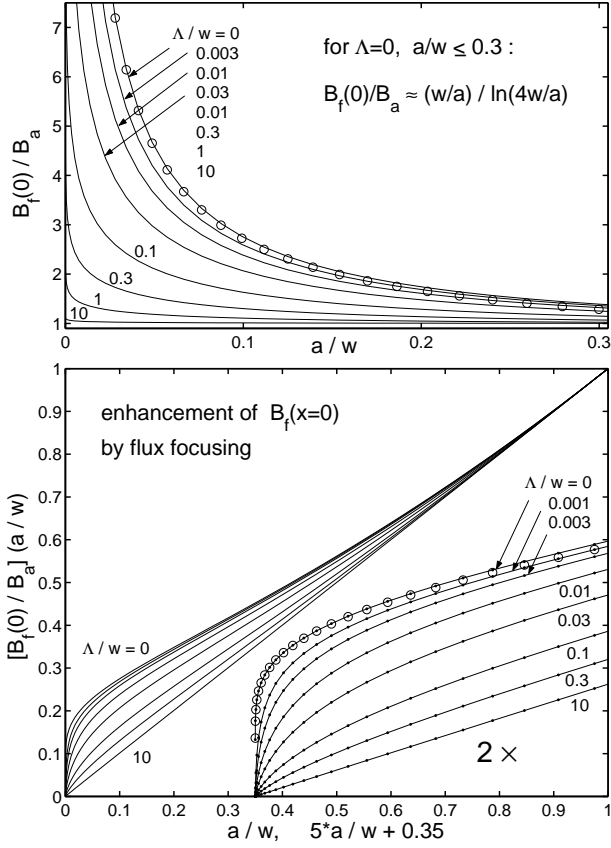


FIG. 15: The minimum of the magnetic induction in the *flux-focusing case*, $B_f(0) = B_f(x=0)$, referred to the applied field B_a and plotted versus the half gap width a/w . Top: The ratio $B_f(x=0)/B_a$, tending to unity for $a/w \rightarrow 1$ and for $\Lambda/w \gg 1$, and diverging for $a/w \rightarrow 0$ when $\Lambda = 0$. Bottom: The same ratio multiplied by a/w to avoid this divergence and fit all data into one plot. The lower right plot depicts the small-gap data two times enlarged along the ordinate, and shifted and five times stretched along the abscissa. The circles show the approximation $B_f(0)/B_a \approx (w/a)/\ln(4w/a)$ good for $a/w \leq 0.3$.⁴⁶

0.1, 0.3, and 1. The first term in Eq. (62) equals the circulating-current sheet-current density, Eq. (54), with appropriate weight factor such that the total circulating current vanishes, $I_1 = I_2 = 0$. The corresponding magnetic field lines are depicted in Fig. 12. Shown in Figs. 13 and 14 are plots of the effective area $A_{\text{eff}}(a/w, \Lambda/w)$ versus a/w and Λ/w , respectively, in units of the maximum possible area $2wl$. In the limit $\Lambda/w \rightarrow 0$, A_{eff} is given by Eq. (A19), and when $\Lambda/w \rightarrow \infty$, $A_{\text{eff}} = l(w+a)$. Note in Fig. 14 that A_{eff} increases with increasing Λ , particularly for small gap widths $2a$. Flux focusing is reflected by the fact that for small $a/w \rightarrow 0$ the effective area A_{eff} of the gap tends to a constant, except in the limit $\Lambda \rightarrow 0$, where it vanishes very slowly, $A_{\text{eff}}/2wl \approx (\pi/2)/\ln(4w/a)$ [Eq. (A19)]. When $a/w \rightarrow 0$, the enhancement factor $A_{\text{eff}}/2al \rightarrow \infty$ and thus diverges even for $\Lambda = 0$. In the limit $a/w \ll 1$, $A_{\text{eff}}(0, \Lambda/w)$ tends to

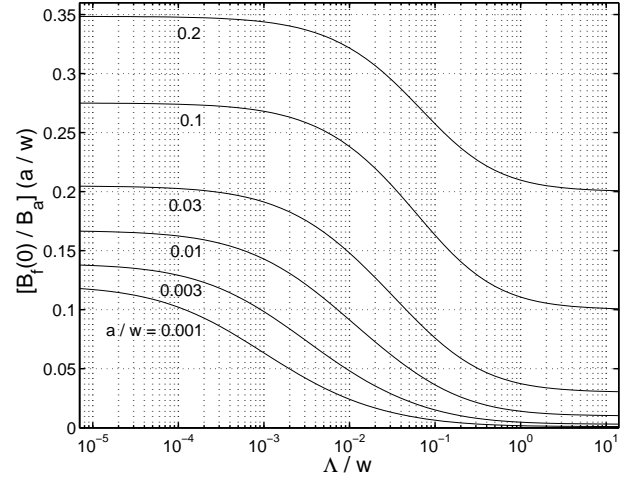


FIG. 16: The minimum field $B_f(0) = B_f(x=0)$ for the *flux-focusing case* as in Fig. 15 but plotted versus Λ/w (range $7 \cdot 10^{-6}$ to 14) for several values of $a/w = 0, 0.001, 0.003, 0.01, 0.03, 0.1$, and 0.2 .

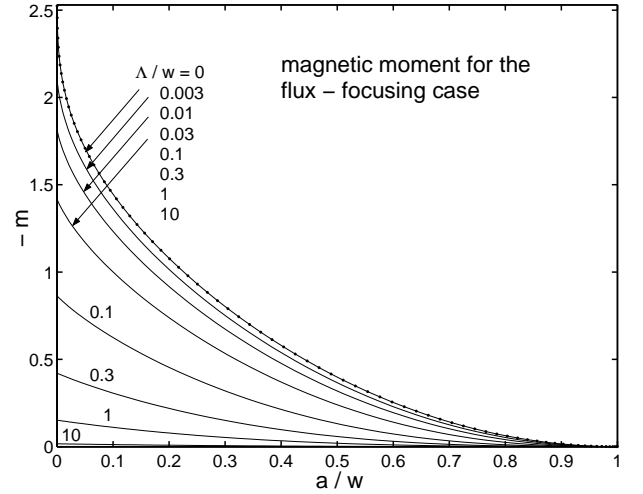


FIG. 17: The magnetic moment m_f for the *flux-focusing case* plotted versus a/w for various values of Λ/w in units $w^2 l B_a / \mu_0$.

a universal function [see Fig. 14]. Interestingly, Figs. 13 and 10 show identical curves; this is because the identity $A_{\text{eff}} = m_d/I_d$ holds for all values of a/w and Λ/w , as proved in general in Sec. II.

Figures 15 and 16 show the minimum of the magnetic induction in the *flux-focusing case*, $B_f(0) = B_f(x=0)$ [see Fig. 11], plotted versus a/w and Λ/w , respectively. The ratio $B_f(0)/B_a \geq 1$ tends to unity for $a/w \rightarrow 1$ and for $\Lambda/w \gg 1$, and it diverges for $a/w \rightarrow 0$ when $\Lambda = 0$. The curve for $\Lambda = 0$ exactly coincides with the analytic expression $B_f(0)/B_a = w\mathbf{E}(k')/a\mathbf{K}(k')$ obtained from Eq. (A17). For $a/w \ll 1$ this yields $B_f(0)/B_a \approx (w/a)/\ln(4w/a)$, which is a good approximation for $0 < a/w \leq 0.3$.⁴⁶ The magnetic moment m_f for the flux-focusing case, calculated from Eq. (60) but

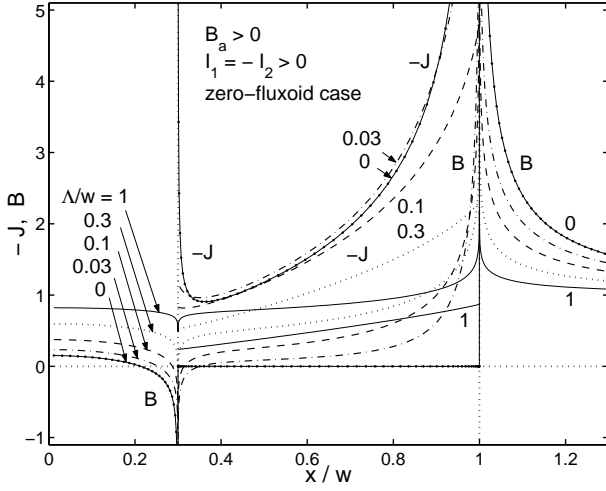


FIG. 18: Profiles of the sheet-current density $J(x)$ [second term in Eq. (62)] and magnetic induction $B(x)$ generated when a perpendicular magnetic induction B_a is applied in the *zero-fluxoid case* when $\Phi = 0$, $I_1 = -I_2 > 0$, and $I = 0$. Shown are the examples $a/w = 0.3$ with $\Lambda/w = 0$ (solid lines with dots), 0.03 (dot-dashed lines), 0.1 (dashed lines), 0.3 (dotted lines), and 1 (solid lines). B and $\mu_0 J$ are in units B_a .

with $J_d(x_i)$ replaced by $J_f(x_i)$, is shown in Fig. 17. Expressions for m_f in the limits $\Lambda/w \rightarrow 0$ and $\Lambda/w \rightarrow \infty$ are given in Eqs. (A20) and (C9)

Shown in Fig. 18 are profiles for the *zero-fluxoid case* with plots of $J(x)$ and the corresponding $B(x)$ generated by an applied magnetic induction $B_a > 0$ when the junctions are short-circuited such that $\Phi = 0$ and $I_1 = -I_2 > 0$; for comparison see analogous profiles in Sec. 2.5 of Ref. 47 for two parallel strips and in Sec. IV of Ref. 48 and Sec. 4 of Ref. 31 for rings. That the current density $J(x)$ in the zero-fluxoid case is given by the second term on the right-hand sides of Eqs. (41) and (62), can be seen by setting $\Phi_f = B_a A_{\text{eff}} = 0$ in Eqs. (40), (41), (61), and (62). Depicted in Fig. 18 are the examples $a/w = 0.3$ with $\Lambda/w = 0, 0.03, 0.1, 0.3$, and 1. Figure 19 shows the magnetic field lines for this case and Fig. 20 the magnetic moment m . Expressions for J , B , and m for the zero-fluxoid case in the limits $\Lambda/w \rightarrow 0$ and $\Lambda/w \rightarrow \infty$ are given in Appendixes A and C.

IV. SUMMARY

In Sec. II of this paper we have presented general equations governing the static behavior of a thin-film dc SQUID for all values of the Pearl length $\Lambda = \lambda^2/d$, where the London penetration depth λ is larger than d , the film thickness. The SQUID's critical current I_c depends upon the effective flux Φ , which is the sum of the magnetic flux up through a contour surrounding the central hole and a term proportional to the line integral of the current density around this contour. For a symmetric SQUID there are three important contributions to Φ : a

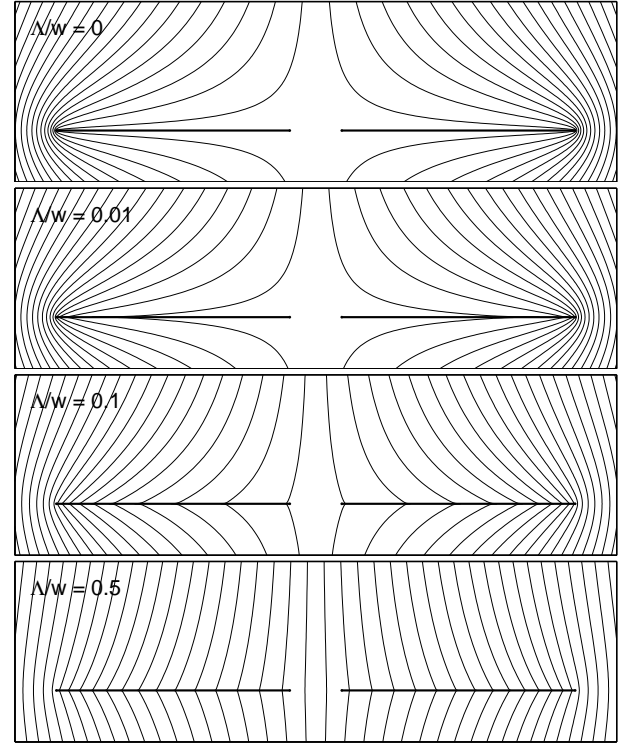


FIG. 19: Magnetic field lines in the *zero-fluxoid case* $\Phi = 0$, $B_a > 0$, and $I = 0$ for $a/w = 0.1$ and $\Lambda/w = 0, 0.01, 0.1$, and 0.5.

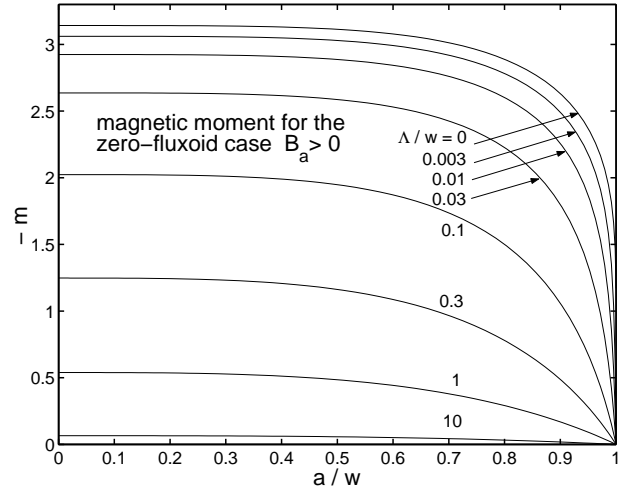


FIG. 20: The magnetic moment m for the *zero-fluxoid case* $\Phi = 0$, $B_a > 0$, and $I = 0$ plotted versus a/w for various values of Λ/w in units $w^2 l B_a / \mu_0$. At $a = \Lambda = 0$ one has $-m = \pi w^2 l B_a / \mu_0$.

circulating-current term Φ_d , a vortex-field term Φ_v , and a flux-focusing term Φ_f , all of which depend upon Λ . Since Λ is a function of temperature, an important consequence is that all of the contributions to Φ are temperature-dependent.

The circulating-current term Φ_d can be expressed in

terms of the SQUID inductance L and the circulating current I_d via $\Phi_d = LI_d$. The SQUID inductance has two contributions, $L = L_m + L_k$, where the first term is the geometric inductance (associated with the energy stored in the magnetic field) and the second is the kinetic inductance (associated with the kinetic energy of the circulating supercurrent). Both contributions are functions of Λ , since they both depend on the spatial distribution of the current density. However, L_m depends only weakly upon Λ , because for the same circulating current I_d , the energy stored in the magnetic field does not vary greatly as Λ ranges from zero to infinity. On the other hand, because the kinetic energy density is proportional to Λ , L_k is also nearly proportional to Λ , with deviations from linearity occurring only for small values of Λ/w .

The vortex-field term can be written as $\Phi_v = \phi_0 G_d$, where G_d is a dimensionless stream function describing the circulating sheet-current density \mathbf{J}_d . Roughly speaking, when Λ is small, I_c is most strongly dependent upon the vortex position when the vortex is close to the edges of the film, but when Λ is large, I_c is equally sensitive to the vortex position wherever the vortex is. Recent experiments⁴⁹ have used the relationship $\Phi_v = \phi_0 G_d$ to determine the vortex-free sheet-current density $\mathbf{J}_d(x, y)$ from vortex images obtained via low-temperature scanning electron microscopy.^{6,9} The experimental data obtained in magnetic fields up to 40 μT are in excellent agreement with numerical calculations of $\mathbf{J}_d(x, y)$, confirming the validity of the above relationship, even in the presence of many (up to 200) vortices in the SQUID washer.

The flux-focusing term can be expressed as $\Phi_f = B_a A_{\text{eff}}$, where B_a is the applied magnetic induction and A_{eff} is the effective area of the central hole of the SQUID. Although A_{eff} is primarily determined by the dimensions of the SQUID, it also depends upon the value of Λ .

To illustrate the Λ dependence of the above quantities, in Sec. III of this paper we analyzed in detail the behavior of a long SQUID whose central region resembles a coplanar stripline. We numerically calculated the profiles of the sheet-current density, stream function, and magnetic induction in the equal-current, circulating-current, flux-focusing, and zero-fluxoid cases for various representative values of Λ . We presented plots of the inductances L , L_m , and L_k , the effective area A_{eff} , and the magnetic moments for these cases. Useful analytic approximations are provided for the $\Lambda/w \rightarrow 0$ limit in Appendix A, for small Λ/w and a/w in Appendix B, and for the $\Lambda/w \rightarrow \infty$ limit in Appendix C.

We are in the process of applying the above theory to square and circular SQUIDS, using the numerical method of Ref. 50.

Acknowledgments

We thank D. Koelle for stimulating discussions. This work was supported in part by Iowa State University

of Science and Technology under Contract No. W-7405-ENG-82 with the U.S. Department of Energy and in part by the German Israeli Research Grant Agreement (GIF) No G-705-50.14/01.

APPENDIX A: THE LIMIT $\Lambda/w = 0$

In the *ideal-screening limit* $\Lambda/w = 0$, the y component of the sheet-current density in the strips ($a < |x| < w$) for the *equal-current case* is⁴⁷

$$J_I(x) = \frac{I}{\pi} \frac{|x|}{[(x^2 - a^2)(w^2 - x^2)]^{1/2}}, \quad (\text{A1})$$

and the z component of the magnetic induction in the plane $z = 0$ of the strips is

$$B_I(x) = -\frac{\mu_0 I}{2\pi} \frac{x}{[(x^2 - a^2)(x^2 - w^2)]^{1/2}}, \quad |x| > w, \quad (\text{A2})$$

$$= 0, \quad a < |x| < w, \quad (\text{A3})$$

$$= \frac{\mu_0 I}{2\pi} \frac{x}{[(a^2 - x^2)(w^2 - x^2)]^{1/2}}, \quad |x| < a, \quad (\text{A4})$$

and the constant C in Eqs. (24), (25), (27), and (28) is $C = \sqrt{w^2 - a^2}/2$.

For the *circulating-current case*, the y component of the sheet-current density in the strips ($a < |x| < w$) in the limit $\Lambda/w = 0$ is⁴⁷

$$J_d(x) = \frac{2B_0}{\mu_0} \frac{x}{|x|} \frac{w^2}{[(x^2 - a^2)(w^2 - x^2)]^{1/2}}, \quad (\text{A5})$$

and the z component of the magnetic induction in the plane $z = 0$ of the strips is

$$B_d(x) = -B_0 \frac{w^2}{[(x^2 - a^2)(x^2 - w^2)]^{1/2}}, \quad |x| > w, \quad (\text{A6})$$

$$= 0, \quad a < |x| < w, \quad (\text{A7})$$

$$= B_0 \frac{w^2}{[(a^2 - x^2)(w^2 - x^2)]^{1/2}}, \quad |x| < a, \quad (\text{A8})$$

where the parameter B_0 , the magnetic flux Φ_d in the z direction in the slot, the circulating current I_d , and the geometric inductance L_m are related by

$$\Phi_d = L_m I_d = 2B_0 l w \mathbf{K}(k) \quad (\text{A9})$$

and

$$L_m = \mu_0 l \mathbf{K}(k) / \mathbf{K}(k'), \quad (\text{A10})$$

where $\mathbf{K}(k)$ is the complete elliptic integral of the first kind of modulus $k = a/w$ and complementary modulus $k' = \sqrt{1 - k^2}$. The geometric inductance is well approximated for small a/w by

$$L_m = (\pi \mu_0 l / 2) / \ln(4w/a), \quad (\text{A11})$$

neglecting corrections proportional to a^2/w^2 , and for small $(w-a)/w$ by

$$L_m = (\mu_0 l / \pi) \ln[16/(1-a^2/w^2)], \quad (\text{A12})$$

neglecting corrections proportional to $1-a^2/w^2$. In the limit that $\Lambda = 0$, the kinetic inductance vanishes ($L_k = 0$), and the inductance in Eq. (A10) becomes the total inductance: $L = L_m$. The magnetic moment [see Eq. (39)] can be obtained from Eqs. (13)-(16) of Ref. 47:

$$m_d = [\pi l w / \mathbf{K}(k')] I_d. \quad (\text{A13})$$

For the *flux-focusing case*, the y component of the sheet-current density in the strips ($a < |x| < w$) in the limit $\Lambda/w = 0$ is⁴⁷

$$J_f(x) = \frac{2B_a}{\mu_0 \mathbf{K}(k')} \frac{x}{|x|} \frac{\mathbf{E}(k')w^2 - 2\mathbf{K}(k')x^2}{[(x^2 - a^2)(w^2 - x^2)]^{1/2}}, \quad (\text{A14})$$

and the z component of the magnetic induction in the plane $z = 0$ of the strips is

$$B_f(x) = -\frac{B_a}{\mathbf{K}(k')} \frac{\mathbf{E}(k')w^2 - 2\mathbf{K}(k')x^2}{[(x^2 - a^2)(x^2 - w^2)]^{1/2}}, \quad (\text{A15})$$

$$|x| > w, \quad (\text{A15})$$

$$= 0, \quad a < |x| < w, \quad (\text{A16})$$

$$= \frac{B_a}{\mathbf{K}(k')} \frac{\mathbf{E}(k')w^2 - 2\mathbf{K}(k')x^2}{[(a^2 - x^2)(w^2 - x^2)]^{1/2}}, \quad (\text{A17})$$

where $\mathbf{E}(k')$ is the complete elliptic integral of the second kind of complementary modulus $k' = \sqrt{1-k^2}$ and modulus $k = a/w$. The magnetic flux in the z direction in the slot is

$$\Phi_f = \pi B_a l w / \mathbf{K}(k'), \quad (\text{A18})$$

and the effective area A_{eff} of the slot is

$$A_{\text{eff}} = \Phi_f / B_a = \pi l w / \mathbf{K}(k'). \quad (\text{A19})$$

Note that $A_{\text{eff}} = m_d / I_d$. The magnetic moment generated by $J_f(x)$ is

$$m_f = -\pi l [w^2 + a^2 - 2w^2 \mathbf{E}(k') / \mathbf{K}(k')] B_a / \mu_0. \quad (\text{A20})$$

For the *zero-fluxoid case*, the y component of the sheet-current density in the strips can be obtained from Sec. 2.5 of Ref. 47:

$$J(x) = -\frac{2B_a}{\mu_0} \frac{x}{|x|} \frac{x^2 - [1 - \mathbf{E}(k) / \mathbf{K}(k)]w^2}{[(x^2 - a^2)(w^2 - x^2)]^{1/2}}. \quad (\text{A21})$$

The corresponding z component of the magnetic induction is⁴⁷

$$B(x) = B_a \frac{x^2 - [1 - \mathbf{E}(k) / \mathbf{K}(k)]w^2}{[(x^2 - a^2)(x^2 - w^2)]^{1/2}}, \quad |x| > w, \quad (\text{A22})$$

$$= 0, \quad a < |x| < w, \quad (\text{A23})$$

$$= B_a \frac{[1 - \mathbf{E}(k) / \mathbf{K}(k)]w^2 - x^2}{[(a^2 - x^2)(w^2 - x^2)]^{1/2}}, \quad |x| < a. \quad (\text{A24})$$

The magnetic moment generated by $J(x)$ is

$$m = -\pi l [2w^2 \mathbf{E}(k) / \mathbf{K}(k) - w^2 + a^2] B_a / \mu_0. \quad (\text{A25})$$

APPENDIX B: BEHAVIOR FOR SMALL Λ AND SMALL a

In this section we present some expressions for L , L_k , and L_m that follow from approximating the circulating-current distribution for small values of Λ and a .

When the slot is very narrow ($a/w \ll 1$), we approximate the sheet-current density in the region $a < x < w$ generated by the fluxoid Φ_d via

$$J_d(x) = I_0 \frac{w}{\sqrt{(x^2 - a^2 + \delta^2)(w^2 - x^2 + \delta^2)}}, \quad (\text{B1})$$

where $I_0 = 2\Phi_d / \pi \mu_0 l$ and δ is a quantity of order $\Lambda = \lambda^2/d$ determined as follows. When $l \rightarrow \infty$ and then $a \rightarrow 0$ and $w \rightarrow \infty$, an exact calculation yields for $x > 0$

$$J_y(x) = \frac{2\Phi_d}{\pi \mu_0 l \Lambda} \int_0^\infty \frac{e^{-xt/\Lambda} dt}{t^2 + 1}. \quad (\text{B2})$$

We find $\int_0^b J_y(x) dx = (2\Phi_d / \pi \mu_0 l) \ln(\gamma b / 2\Lambda)$ when $b \gg \Lambda$, where $\gamma = e^C = 1.781\dots$, and $C = 0.577\dots$ is Euler's constant. From Eq. (B1) we find $\int_0^b J_d(x) dx = (2\Phi_d / \pi \mu_0 l) \ln(2b/\delta)$ when $a = 0$ and $\delta \ll b \ll w$. Comparing these two integrals we obtain $\delta = (4/\gamma)\Lambda = 2.246\Lambda$. Integrating Eq. (B1) from a to w to obtain I_d , we find

$$I_d = I_0 \frac{w}{\sqrt{w^2 + \delta^2}} [F(\lambda_a, q) - F(\lambda_w, q)], \quad (\text{B3})$$

where $F(\phi, k)$ is the elliptic integral of the first kind and

$$\lambda_a = \arcsin \sqrt{\frac{w^2 - a^2 + \delta^2}{w^2 - a^2 + 2\delta^2}}, \quad (\text{B4})$$

$$\lambda_w = \arcsin \frac{\delta}{\sqrt{w^2 - a^2 + 2\delta^2}}, \quad (\text{B5})$$

$$q = \sqrt{\frac{w^2 - a^2 + 2\delta^2}{w^2 + \delta^2}}. \quad (\text{B6})$$

Expanding Eq. (B3) for $a \ll w$ and $\delta \ll w$, using $I_0 = 2\Phi_d / \pi \mu_0 l$, and neglecting terms of order a^2/w^2 and δ^2/w^2 , we obtain

$$L = \Phi_d / I_d = (\pi \mu_0 l / 2) / \{\ln[4w/(a + \delta)] - \delta/w\}, \quad (\text{B7})$$

where $\delta = 2.246\Lambda$. Note that Eq. (B7) reduces to Eq. (A11) when $\Lambda = 0$.

From Eq. (B1) we obtain the approximation

$$\int_a^w J_d^2(x) dx = I_0^2 \frac{w}{(w^2 - a^2 + \delta^2)} (f_a + f_w), \quad (\text{B8})$$

where

$$f_a = \frac{w}{\sqrt{\delta^2 - a^2}} \tan^{-1} \frac{(w-a)\sqrt{\delta^2 - a^2}}{a(w-a) + \delta^2}, \quad (\text{B9})$$

$$a < \delta,$$

$$= \frac{w}{\sqrt{a^2 - \delta^2}} \tanh^{-1} \frac{(w-a)\sqrt{a^2 - \delta^2}}{a(w-a) + \delta^2}, \quad (\text{B10})$$

$$a > \delta,$$

$$f_w = \frac{w}{\sqrt{w^2 + \delta^2}} \tanh^{-1} \frac{(w-a)\sqrt{w^2 + \delta^2}}{w(w-a) + \delta^2}. \quad (\text{B11})$$

Using Eqs. (B3) and (B8), we obtain from Eq. (38)

$$L_k = 2\mu_0 l \frac{\Lambda}{w} \frac{(w^2 + \delta^2)}{(w^2 - a^2 + 2\delta^2)} \frac{(f_a + f_w)}{[F(\lambda_a, q) - F(\lambda_w, q)]^2}, \quad (\text{B12})$$

where $\delta = 2.246\Lambda$. Although our intention in using the ansatz of Eq. (B1) initially was to obtain an improved approximation to L_k for small values of Λ and a , we see from Figs. 8(b) and 9(b) that Eq. (B12) provides a reasonably good approximation for all values of Λ and a .

APPENDIX C: THE LIMIT $\Lambda/w \rightarrow \infty$

In the *weak-screening limit* $\Lambda/w \rightarrow \infty$, $K^{\text{sy}}(x, x') = \Lambda^{-1}\delta(x - x')$, the y component of the sheet-current density in the strips ($a < |x| < w$) in the *equal-current case* is uniform, $J_I = I/2(w - a)$, the z component of the magnetic induction in the plane of the strips obtained from the Biot-Savart law is

$$B_I(x) = \frac{\mu_0 I}{4\pi(w - a)} \ln \left| \frac{(x - w)(x + a)}{(x + w)(x - a)} \right|, \quad (\text{C1})$$

and the constant C in Eqs. (24), (25), (27), and (28) is $C = w \exp[-\pi\Lambda/(w - a)]$.

For the *circulating-current case* in the limit $\Lambda/w \rightarrow \infty$, $K^{\text{as}}(x, x') = \Lambda^{-1}\delta(x - x')$, $\alpha = \Lambda/(w - a)$, the y component of the sheet-current density in the strips is again uniform, $J_d = I_d/(w - a)$ for $a < x < w$, and the z component of the magnetic induction in the plane of the strips obtained from the Biot-Savart law is

$$B_d(x) = \frac{\mu_0 I_d}{2\pi(w - a)} \ln \left| \frac{x^2 - w^2}{x^2 - a^2} \right|. \quad (\text{C2})$$

The geometric inductance is, from Eq. (37)

$$L_m = \frac{\mu_0 l}{\pi(w - a)^2} \left[w^2 \ln \left(\frac{4w^2}{w^2 - a^2} \right) - 2aw \ln \left(\frac{w + a}{w - a} \right) + a^2 \ln \left(\frac{4a^2}{w^2 - a^2} \right) \right], \quad (\text{C3})$$

which is independent of Λ . Equation (C3) is well approximated for small a/w by

$$L_m = (\mu_0 l/\pi)(1 + 2a/w) \ln 4, \quad (\text{C4})$$

neglecting corrections proportional to a^2/w^2 , and for small $(w - a)/w$ by

$$L_m = (\mu_0 l/\pi) \left[\ln \frac{2}{1 - a/w} + \frac{3}{2} - \frac{1}{2}(1 - a/w) \right], \quad (\text{C5})$$

neglecting corrections proportional to $(1 - a/w)^2$. From Eq. (38) we obtain the kinetic inductance

$$L_k = 2\mu_0 l \Lambda / (w - a). \quad (\text{C6})$$

When $\Lambda \gg w$, the total inductance L is dominated by the kinetic inductance ($L_k \gg L_m$), such that $L \approx L_k$. Since J_d is uniform, the magnetic moment is easily found from Eq. (39) to be

$$m_d = l(w + a)I_d. \quad (\text{C7})$$

For the *flux-focusing case* in the limit $\Lambda/w \rightarrow \infty$, $K^{\text{as}}(x, x') = \Lambda^{-1}\delta(x - x')$, the y component of the sheet-current density is $J_f(x) = B_a(w + a - 2x)/2\mu_0\Lambda$ for $a < x < w$, the effective area is $A_{\text{eff}} = l(w + a) = m_d/I_d$, and the z component of the magnetic induction in the plane of the strips is $B_f(x) = B_a + B_{\text{sf}}(x)$, where from the Biot-Savart law

$$B_{\text{sf}}(x) = \frac{B_a}{4\pi\Lambda} \left[(w + a) \ln \left| \frac{x^2 - w^2}{x^2 - a^2} \right| + 2x \ln \left| \frac{(x + w)(x - a)}{(x - w)(x + a)} \right| - 4(w - a) \right]. \quad (\text{C8})$$

The magnetic moment generated by $J_f(x)$ in this limit is

$$m_f = -[l(w - a)^3/6\Lambda](B_a/\mu_0). \quad (\text{C9})$$

For the *zero-fluxoid case* in the limit $\Lambda/w \rightarrow \infty$, the applied field is only weakly screened, and the z component of the magnetic flux density is nearly equal to the applied magnetic induction, $B(x) \approx B_a$. The y component of the vector potential is approximately given by $A(x) = B_a x$, and the y component of the induced sheet-current density, obtained from Eq. (1) with $\gamma = 0$, is $J(x) = -(B_a/\mu_0\Lambda)x$. To the next order of approximation, $B(x) = B_a + B_s(x)$, where the self-field B_s is found from the Biot-Savart law

$$B_s(x) = \frac{B_a}{2\pi\Lambda} \left[x \ln \left| \frac{(x + w)(x - a)}{(x - w)(x + a)} \right| - 2(w - a) \right]. \quad (\text{C10})$$

The magnetic moment generated by $J(x)$ in this limit is

$$m = -[2l(w^3 - a^3)/3\Lambda](B_a/\mu_0). \quad (\text{C11})$$

¹ See the review by D. Koelle, R. Kleiner, F. Ludwig, E. Dantsker, and J. Clarke, Rev. Mod. Phys. **71**, 631 (1999), and references therein.

² M. J. Ferrari, J. J. Kingston, F. C. Wellstood, and J. Clarke, Appl. Phys. Lett. **58**, 1106 (1991).

³ A. H. Miklich, D. Koelle, T. J. Shaw, F. Ludwig, D. T.

- Nemeth, E. Dantsker, J. Clarke, N. McN. Alford, T. W. Button, and M. S. Colclough, *Appl. Phys. Lett.* **64**, 3494 (1994).
- ⁴ V. N. Glyantsev, Y. Tavrín, W. Zander, J. Schubert, and M. Siegel, *Supercond. Sci. Technol.* **9**, A105 (1996).
- ⁵ R. G. Humphreys, *IEEE Trans. Appl. Supercond.* **9**, 3741 (1999).
- ⁶ R. Straub, S. Keil, R. Kleiner, and D. Koelle, *Appl. Phys. Lett.* **78**, 3645 (2001).
- ⁷ R. Wördenweber, P. Lahl, and P. Dymashevski, *Physica C* **369**, 141 (2002).
- ⁸ S. Kuriki, Y. Kawaguchi, K. Takahashi, and M. Matsuda, *J. Appl. Phys.* **96**, 2768 (2004).
- ⁹ D. Doenitz, R. Straub, R. Kleiner, and D. Koelle, *Appl. Phys. Lett.* **85**, 5938 (2004).
- ¹⁰ E. R. Nowak, *Physica C* **421**, 15 (2005).
- ¹¹ J. R. Clem, "Vortex exclusion from superconducting strips and SQUIDS in weak perpendicular ambient magnetic fields," unpublished.
- ¹² E. Dantsker, S. Tanaka, P.-Å. Nilsson, R. Kleiner, and J. Clarke, *Appl. Phys. Lett.* **69**, 4099 (1996).
- ¹³ E. Dantsker, S. Tanaka, and J. Clarke, *Appl. Phys. Lett.* **70**, 2037 (1997).
- ¹⁴ E. E. Mitchell, D. L. Tilbrook, J. C. MacFarlane, and C. P. Foley, *IEEE Trans. Appl. Supercond.* **13**, 849 (2003).
- ¹⁵ G. Stan, S. B. Field, and J. M. Martinis, *Phys. Rev. Lett.* **92**, 097003 (2004).
- ¹⁶ J. Du, D. L. Tilbrook, J. C. MacFarlane, K. E. Leslie, D. S. Ore, *Physica C* **411**, 18 (2004).
- ¹⁷ J. Pearl, *Appl. Phys. Lett.* **5**, 65 (1964).
- ¹⁸ F. London, *Superfluids*, Vol. 1 (Dover, New York, 1961).
- ¹⁹ We use the subscript d as a reminder that I_d is just the difference between $I_2/2$ and $I_1/2$.
- ²⁰ M. B. Ketchen, W. J. Gallagher, A. W. Kleinsasser, S. Murphy, and J. R. Clem, in *SQUID '85, Superconducting Quantum Interference Devices and their Applications*, edited by H. D. Hahlbohm and H. Lübbig (de Gruyter, Berlin, 1985), p. 865.
- ²¹ T. P. Orlando and K. A. Delin, *Foundations of Applied Superconductivity* (Addison-Wesley, Reading, 1991).
- ²² B. D. Josephson, in *Superconductivity*, Vol. 1, edited by R. D. Parks, (Dekker, New York, 1969), p. 423.
- ²³ J. D. Jackson, *Classical Electrodynamics*, (Wiley, New York, 1962).
- ²⁴ R. de Bruyn Ouboter and A. Th. A. M. de Waele, in *Progress in Low Temperature Physics*, Vol. VI, edited by C. J. Gorter (North-Holland, 1970), Chap. 6.
- ²⁵ L. Solymar, *Superconductive Tunneling and Applications*, (Wiley, New York, 1972).
- ²⁶ R. de Bruyn Ouboter, in *Superconductor Applications: SQUIDS and Machines*, edited by B. B. Schwartz and S. Foner (Plenum, New York, 1977), Chap. 2.
- ²⁷ T. Van Duzer and C. W. Turner, *Principles of Superconductive Devices and Circuits*, (Elsevier, New York, 1981).
- ²⁸ J. Clarke, in *Superconducting Devices*, edited by S. T. Ruggerio and D. A. Rudman, (Academic Press, San Diego, 1990), Chap. 2.
- ²⁹ M. Tinkham, *Introduction to Superconductivity*, (McGraw-Hill, New York, 1996).
- ³⁰ Throughout this paper a lower-case j denotes a current density (current per unit area) and an upper-case J denotes a sheet-current density (current per unit width).
- ³¹ E. H. Brandt and J. R. Clem, *Phys. Rev. B* **69**, 184509 (2004).
- ³² This equation corresponds to the identity $\alpha_m = \beta_l$ found for superconducting rings in Ref. 31.
- ³³ A similar relation between the vortex-generated flux and the stream function was derived by Humphreys in Ref. 5 using inductance arguments.
- ³⁴ J. R. Clem *Phys. Rev. B* **1**, 2140 (1970).
- ³⁵ J. Z. Sun, W. J. Gallagher, and R. H. Koch, *Phys. Rev. B* **50**, 13664 (1994).
- ³⁶ C. M. Pegrum, A. Eulenburg, E. J. Romans, C. Carr, A. J. Millar, and G. B. Donaldson, *Supercond. Sci. Technol.* **12**, 766 (1999).
- ³⁷ A. Eulenburg, E. J. Romans, C. Carr, A. J. Millar, G. B. Donaldson, and C. M. Pegrum, *Appl. Phys. Lett.* **75**, 2301 (1999).
- ³⁸ S. Kuriki, H. Oyama, E. Maruyama, A. Hayashi, S. Hirano, D. Suzuki, and M. Koyanagi, *IEEE Trans. Appl. Supercond.* **9**, 3275 (1999).
- ³⁹ E. E. Mitchell, D. L. Tilbrook, C. P. Foley, and J. C. MacFarlane, *Appl. Phys. Lett.* **81**, 1282 (2002).
- ⁴⁰ E. H. Brandt, *Phys. Rev. B* **64**, 024505 (2001).
- ⁴¹ E. H. Brandt, *Phys. Rev. B* **49**, 9024 (1994).
- ⁴² E. H. Brandt, *J. de Physique C8*, 31 (1987).
- ⁴³ The accuracy of this sum (error $\propto 1/N$) is improved (error $\propto 1/N^2$) by multiplying the last term $j = i$ with $1/2$. Even higher accuracy can be reached by interpolation, using different weights for each i that vanish at the boundaries (a, x_i) of the indefinite integral.
- ⁴⁴ K. Yoshida, M. S. Hossain, T. Kisu, K. Enpuku, and K. Yamafuji, *Jpn. J. Appl. Phys.* **31**, 3844 (1992).
- ⁴⁵ R. Meservey and P. M. Tedrow, *J. Appl. Phys.* **40**, 2028 (1969).
- ⁴⁶ G. P. Mikitik and E. H. Brandt, *Phys. Rev. B* **64**, 092502 (2001).
- ⁴⁷ A. A. Babaei Brojeny, Y. Mawatari, M. Benkraouda, and J. R. Clem, *Supercond. Sci. Technol.* **15**, 1454 (2002).
- ⁴⁸ A. A. Babaei Brojeny and J. R. Clem, *Phys. Rev. B* **68**, 174514 (2003).
- ⁴⁹ D. Doenitz, M. Ruoff, E. H. Brandt, J. R. Clem, R. Kleiner, and D. Koelle, unpublished.
- ⁵⁰ E. H. Brandt, *Phys. Rev. B* **72**, 024529 (2005).